ABSTRACT

CHENGXI, LI. Process Optimization in Unconfined Melt Electrospinning with a Focus on Ambient Conditions. (Under the direction of Drs. Russell Gorga and Laura Clarke).

Ultrafine fibers are fibers with a small diameter. Because of the unique character that they have a high surface area to volume ratio, they are performing many unique properties in air filtration, tissue engineering, biomedical applications.

There are various methods to make the ultrafine fibers and electrospinning has been a popular way for decades. Electrospinning is a method that applies the high voltage to the polymer solution or molten polymer. If there is an area with sufficient high electric field intensity, the repellent force between molecules will overcome the surface tension of the liquid source material and initiate a fiber which will be attracted to the collector where is at lower electric potential. However, most studies are based on solution electrospinning and seldom of them discuss melt electrospinning. There are a lot of advantages of solution electrospinning such as easy to prepare the materials, simple setups, and the proven ability to make nanofibers. However, there are certain restrictions which make melt electrospinning attractive such as some polymers are hard to dissolve, especially the very popular materials in the textile industry, e.g. polyethylene and polypropylene. On the other hand, there is an upper limit in diameter for solution electrospinning. The fiber foaming process in solution electrospinning relies on the evaporation of solvent during the journey from the initiator to the collector. If the jet volume is too large, the fiber will not “dry” before it reaches to the collector. Needless to say the difficulty of making high percentage polymer solution and pollution concerns exist about volatile solvents.

Melt electrospinning could potentially solve those two problems but also has other challenges. Due to the high viscosity of polymer melt, it becomes harder to produce fine fibers. The temperature control also must precise otherwise the molten polymer will clog the nozzle inside the needle. Needleless melt electrospinning is a method to solve the clogging problems but still needs a lot of research efforts to produce the ultrafine melt electrospun fibers. This work is part of a big project to study the mechanism of melt electrospinning and to find better solutions for making smaller fibers directly from molten polymers. This work contains a series of optimizations to the initial setup, decreased the diameter of fibers to the 10% of the previous work by increased the working electric field intensity without changing any voltage and distance. The study also focuses on the ambient conditions, analyzing the correlations between ambient temperatures, spinning area air flow, spinning distance affect to the spinning process.

Process Optimization in Unconfined Melt Electrospinning with a Focus on Ambient Conditions.

by
Chengxi Li

A thesis submitted to the Graduate Faculty of
North Carolina State University
in partial fulfillment of the
requirements for the degree of
Master of Science

Textile Engineering

Raleigh, North Carolina
2018

APPROVED BY:

Dr. Russell Gorga Committee Co-Chair	Dr. Laura Clarke Committee Co-Chair
Dr. Jason Bochinski	Dr. Wendy Krause

BIOGRAPHY

Chengxi Li was born in Hefei, China. He received his Bachelor of Engineering degree in Textile Engineering from Donghua University at Shanghai, China in 2016 and a minor degree in Applied Psychology from East China Normal University at Shanghai, China in the same year. He was in Dr. Qiuran Jiang's research group studying about electrospun ultrafine conductive air filter.

During the master's degree program at North Carolina State University, he works with Dr. Russell Gorga and Dr. Laura Clarke in the direction of melt electrospinning system optimization.

ACKNOWLEDGMENTS

The project is funded by US National Science Foundation, Grant number 1462966.

Great appreciation to my advisors Dr. Russell Gorga, Dr. Laura Clarke and Dr. Jason Bochinski for the instructions.

Many thanks to my group member, Ms. Elnaz Shabani, for sharing the ideas, suggestions and the cooperating works.

Thanks Ms. Judy Elson and Mr. Chuck Mooney for the instrument training and Mr. Geoffrey Scott for the engineering supports.

TABLE OF CONTENTS

LIST OF FIGURES

LIST OF TABLES

1. INTRODUCTION

1.1. Nanofibers and mesofibers

Ultrafine fibers refers to fibrous material with diameters from 1 nm to 100 microns. This kind of fiber shows a large surface area to volume ratio, good flexibility and small pores size than larger fibers in nonwoven mats. It is a popular topic in the materials and textiles research area. There are many applications that utilize the features of ultrafine fibers. Air filtration (Hung and Leung 2011) is a good example. Not all the particles in the air is troublesome to people. For large particles like dust, simply using a sponge as the vacuum cleaner filter is effective enough. However, for the particles of some certain small size, usually from 2.5 microns (PM2.5) to 10 micron (PM10), the filter made by common textile fibers cannot stop and hold such small particles and requires smaller fibers. Once the fiber gets thinner, the pressure-drop of the airflow going through the filter is decreased as well, which means a less energy consumption. Tissue scaffold (Cai et al. 2013) and drug delivery (Hu et al. 2014) are some important applications in the biomedical field. The scaffold made by fibers of hundreds nanometer in diameter is very similar to the cytoplasmic matrix. The tissue is better to grow on the similar material as the original environment to minimize the rejection reaction. Ultrafine fibers could also be used as the enhancement material for composites with a super light weigh percent. A study placed polybenzimidazole (PBI) nanofibers in rubber and epoxy matrix (Kim and Reneker 1999). The PBI fiber was directly spun onto the laminates when preparing the composites materials and then covered the laminates with rubber. The fibers are only 3-15 wt % in this study and the Young's modulus increased to 10 times and the tear strength increased 100%.

There are other more interesting applications of ultrafine fibers and many of them are related with mechanical properties. Although a strand of microfibers may be stronger than a single fiber at the same cross-section area because of the inter fibers friction (Schmid et al. 2000), the single thinner fiber is always weak. When the application requires a higher mechanical property, the middle size fibers might work better than the ultrafine fibers to reduce the stability concern. The fiber ranged between 0.5 and 4.5 μm are named meso-fibers in some studies (Hoffstetter and Wintermantel 2010). Their study is using the mesofibers as the reinforce microparts.

1.2. The methods of making ultrafine fibers

Electrospinning refers to "electrostatic spinning" which is a method of spinning fibers with a history over a hundred years (Cooley 1903). At first, it was just a technique to make normal sized fibers. However, due to the non-contact property, electrospinning has been used broadly into generating smaller sized fibers. The current products are ranging from several nanometers to hundreds of microns. Electrospinning is a straightforward and popular way of making ultrafine fibers, however, there are more substitutions, for instance, self-assembly (Kapllani et al. 2014), phase separation (Lv et al. 2015), traditional dry spinning with advanced drawing technics (Ondarcuhu and Joachim 1998; Xing et al. 2008), and template synthesis (Liang et al. 2012).

By simply drawing the molten polymer, it is possible to acquire ultrafine fibers. However, this method requires the precisely controlled drawing force tuning with the viscosity of the polymers otherwise the polymer melt might break while the attenuation process. The reason is that the viscosity of the molten polymer changes when the temperature is reduced and the ultrafine melt polymer jets are very fragile. Hence, the drawing process and the winding are all required to be gentle and stable which is hard for traditional rollers. In the history, mechanical drawing is hard to get polymer fibers less than 1 μm (Brown et al. 2016). Using melt blowing technology, drawing the melt polymer by hot air, is possible to get fibers at several hundred nanometers in diameter but usually for mass production of bonded nonwoven mats with expensive equipment. Self-assembly is a method that the material grows at the end of the existing material. This method is more suitable for making materials with special structure but doesn't have strength in terms of speed and cost. Phase separation is another method of fiber spinning. The common idea is manipulating the solubility of polymer solvent by changing temperature, adding other reduce solubility reactor or pressure change. According to the controlled change, only a small portion of the polymer solute get coagulated, so it is possible to generate ultrafine fibers. It is a combined process with dissolution, gelation, extraction by different solvents but also a time-consuming process. The template synthesis method is an interesting method that a membrane with nano-sized porous is used as a template and the polymer melt will drop thorough the small holes to become to ultrafine fibers. The fiber could be made either solid or hollow. The raw material is broad that even some conducting material is applicable which is not suitable for electrospinning but unable to make one-by-one continuous fiber is a problem.

In conclusion, electrospinning is an effective way to produce ultrafine fibers in a relatively wide range of diameter from various raw materials. The structure of the setup is usually simple and inexpensive. It’s a suitable method, especially for small-scale production.

1.3. Introduction of solution electrospinning

Due to the advantages concluded above, electrospinning has been a hot topic research for decades. To classify electrospinning by the form of source material, it could be categorized in solution electrospinning and melt electrospinning. In solution electrospinning, the polymer is the solute in a solution system and the solution is the raw material. While in melt electrospinning, the polymer itself in the melt status is the raw material. Solution electrospinning has been studied more than the melt electrospinning because it is simple to accomplish and the stable performance of getting sub-micron fibers.

1.3.1. The mechanism of solution electrospinning

Although there are many configurations of solution electrospinning, usually there is a syringe pump containing the polymer solution. The solution has to be charged with high voltage potential by an attached electrode. The high voltage will induce free charges in the solution and moving to the direction at lower voltage potential where is the collector. For the reason that most area of the syringe side is constrained by the wall, the only breakthrough point is the end tip of the needle. Usually, there is a hanging drop due to the pressure of the pump and a cone is going to initiate from the pendant towards the collector. Once the voltage difference is large enough, the electric force will overcome the surface tension of the liquid and a jet of solution will be ejected out.

Different from the ionic solution, the molecules which carrying the charges are relatively hard to move freely. Once it has been pulled out from the main solution body, the charged molecules will be dragged to the collector and the solution is evaporated during that process, leaving a fiber behind. Some dilute solution might break during the drying process for the too strong drawing force and too small self-restriction from the viscosity, so the viscosity is a key parameter in the electrospinning (Subbiah et al. 2005).

The previous demonstrated raw material for solution electrospinning is broad. Many common polymers have been tried before, such as Nylon6, 6, Polyurethanes (PU), Polybenzimidazole (PBI), Polycarbonate (PC), Polyacrylonitrile (PAN), Polyvinyl alcohol (PVA), Polylactic acid (PLA), Polyethylene terephthalate (PET), and Polystyrene (PS) (Huang et al. 2003). There are two essential similar points for those materials. The first is that the polymer must have a good solvent, and the solution stays stable during the spinning process. The second similarity is the evaporation of the solvent must be good so that the solvent is gone before the fiber reaching the collector. The spinning distance is usually only 10-20 cm away.

1.3.2. Unconfined needleless electrospinning

Solution electrospinning, of course, has many restrictions. One that inhibits it from becoming commercialized is its low throughput rate. The traditional single needle setup typically deposits 0.1–1.0 g polymers per hour (Dosunmu et al. 2006). There are several improved methods of the traditional needle solution electrospinning. Making more jets on one nozzle is a group and arranging multiple needles in the electrospinning system is another group. However, clogging is a common concern for solution electrospinning. If the system is fed by multiple channels, preventing the channels being clogged will make the system even more complex.

More needles allowing more jets to spin simultaneously. If applying the differential idea in this engineering problem, the needles could be so small and so close to each other that the small dots are connected into a line. Some studies used this idea to make microfibers before. Bubble electrospinning (Liu and He 2007), is one application that bubbles are induced at the polymer solution surface. The Taylor cones generate at the top of the bubbles to achieve the goal of mass production. Disk electrospinning by (Niu et al. 2009), describes another solution by using a metal disk soaked by polymer solution as the electrode [Figure 1]. Fibers are initiated at the edge facing the collector.

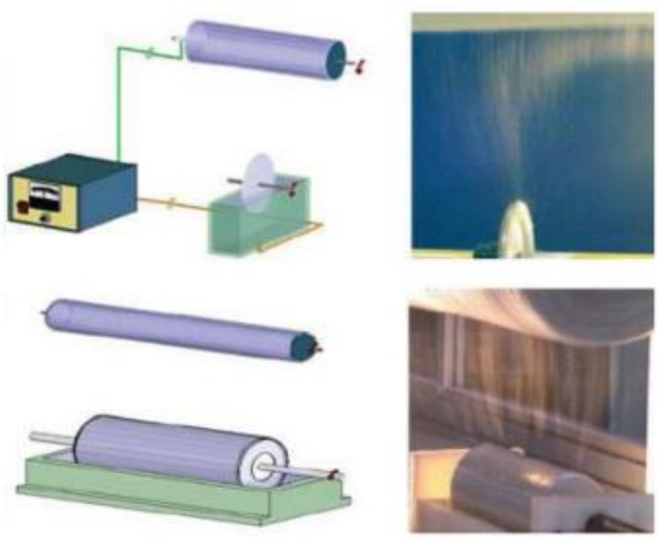

Figure 1. The scheme of a disk solution electrospinning (Niu et al. 2009).

Inspired by the previous needleless and unconfined electrospinning methods, Roman et al. (2013) created an edge unconfined electrospinning system to study the underlined physics principles for the purpose of generalize the needleless method. Their goal is when using various fluid and different electric field, the system should always be able generated microfibers smoothly. This system consists of a plate with three short walls and one side open, a flat metal collector and the fiber is coming out from the open side.

1.4. Introduction of melt electrospinning

Similar to solution electrospinning, melt electrospinning is a process that can producing microfibers. They both include a polymer source feeding system, a collector, and a voltage difference between the two parts. Although melt electrospinning is a similar process as the solution electrospinning, a survey of the literature in May 2010 (ISI Web of Science) estimates that out of 3480 journal articles that include the words "electrospinning" or "electrospun", a total of 24 articles reporting the use of melt electrospinning, which is only 0.7%. The intrinsic reason is the difficulty of getting the as-small fiber comparing to solution electrospinning. To spin fiber from the polymer melt, keeping the temperature of polymer higher than the melting point is necessary. However, most common polymers have the melt point way higher than the room temperature, so it needs to be heated by another part which increased the complexity of the system. Another problem is the fiber formation process. The fibers made by melt electrospinning process is usually 10-100 times thicker than the solution electrospun fibers. One reason is that the polymer solution used in electric spinning usually contains about only 10 wt % polymer solute which means about 90% volume of the jet will disappear during the evaporation process. However, in the melt electrospinning, all volume of the jet is kept as the fiber which requires more effort in the drawing process. The worse factor is the viscosity of polymer melt is usually much higher than the polymer solution so it is harder to be pulled by the relatively weak electric force. Needless to say, as well, the polymer melt might become solidified during the spinning if the ambient temperature is lower than the melting point.

Though there are many difficulties stated above, melt electrospinning has still become a hotter topic in recent years. In the Google Scholar search engine, there are 62,700 papers including “electrospinning” from 2010 to 2018 and 17,600 of them including “melt electrospinning” which is 28.1%. There are two major reasons to develop this method instead of solvent electrospinning. The first reason is that the volatile solvent is a concern when facing strict environmental regulations or meeting the requirement of end users. There are already many microfiber applications in the biomedical area and the food industry, and the need to avoid the residual of the toxic organic solvent like Tetrahydrofuran (THF) or Dimethylformamide (DMF) is something whitch needs to be considered.

Another reason is that some semi-crystalized polymers, for instance, PE, PP are hard to dissolve, and they are widely used in textile, fiber industry. An effective method of making ultrafine fibers of these materials is therefore very worthwhile to study.

1.4.1. The principle of melt electrospinning

A melt electrospinning setup is demonstrated in [Figure 2]. The cone forms at the spinneret, the same as the solution electrospinning. Once the voltage difference is beyond the critical value, the electrostatic energy accumulated in the cone will overcome the surface tension and the viscoelastic property of the molten polymer forms a jet.

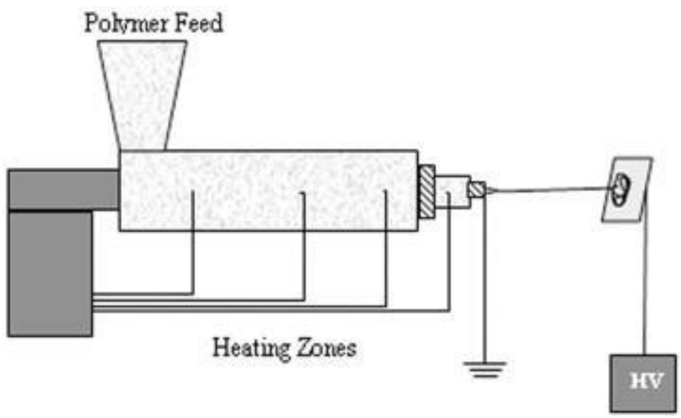

Figure 2. A scheme of a melt needle electrospinning system (Lyons et al. 2004).

If the unstable area (whipping area) does not appear in the melt electrospinning process, there could be two reasons (Lyons et al. 2004). The first one is the spin distance between the nozzle and the collector is not long enough to let the polymer jet performing the whole typical electrospinning process because some experiment setup works only have 3 cm working distance. Another explanation is that the viscosity of the molten polymer is too high as compared to the polymer solution that the electrical force is not large enough to drive the movement.

There are several factors that have been revealed to affect the diameter of the produced fibers. The molecular weight is a key factor that determines the fiber diameter. By the work of W. L. Peticolas and J. M. Watkins (1957), the viscosity of melt Polyethylene at 150 °C is shown in [Figure 3].

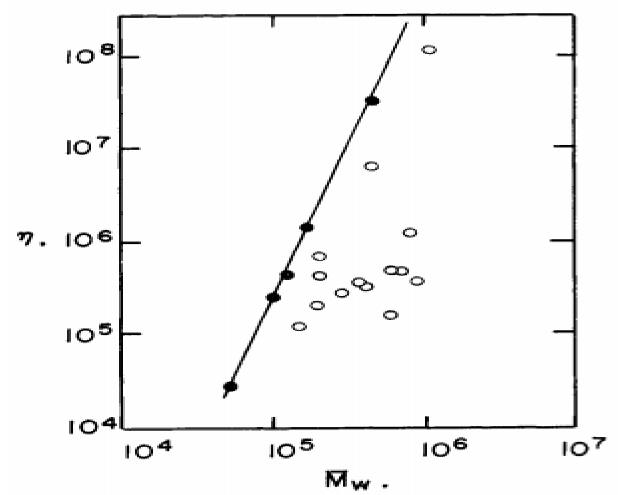

Figure 3. The viscosity of PE as the function of molecular weight. The solid dots are liner polyethylene (PE) and the hollow dots are branch PE. (W. L. Peticolas and J. M. Watkins 1957).

As the data in the [Figure 3], the molecular weight affects the viscosity a lot and acting as the resistance force in the drawing process. At the same drawing force condition, thicker fiber will be produced. The crystallization is another factor that massively increasing the viscosity of the fiber when quenching so the isotactic polymers may produce thicker polymers even the absolute melt viscosity, is relatively low.

1.4.2. The parameters affecting melt electrospinning

According to the orthogonal designed study of the importance of each factor in melt electrospinning by Liu et al. (2010), the sequence from the most important to the least is

Melt Flow Rate (MFR) > spinning temperature > spinning distance > melt temperature.

The sequence is based on the fiber diameter variance range analysis for the orthogonal experiments and the range (R_j) for each parameter is shown below in [Table 1]

Table 1. Range analysis for orthogonal experiments of parameters affecting melt electrospinning (Liu et al. 2010).

parameter	MFR (g/10 min)	voltage (kV)	distance (cm)	temperature (°C)
Rj	49.41	46.16	44.65	41.21

1.4.3. The developments in melt electrospinning

There are many approaches to optimize the melt electrospinning. Near Field Electrospinning (NFES) is an example (Sun et al. 2006). The traditional electrospinning has a spinning distance around 5-50 cm while the near-field electrospinning could be 0.05-5 cm. As a consequence, the applied voltage is lowered to less than 10 kV. This is a good example to reduce the requirement of instruments but the drawing process in the air is important for making ultrafine fibers when electrospinning. Due to the reduced drawing distance, NFES usually produces fibers larger than traditional melt electrospinning.

Inspired by the idea that the viscosity is restricting the production of nano-size fibers, Dalton et al. (2007) conducted experiments by adding 1.5% viscosity-reducing additive Irgatec ® (provided by BASF) , the zero-shear viscosity of the PP-15 melt drop from 75 Pa•s to 33 and the diameter of polypropylene fibers can be reduced from 35 ± 8 μm, to 840 ± 190 nm. This study also tried the combination of PEG47-block-PCL95 + 30% PCL and collected fiber of 0.27 ± 0.10 μm which was the finest fiber compared to previous works.

Despite of reducing the viscosity of polymer melt, increasing the drawing force is another effective way to reduce the fiber diameter. Zhmayev et al. (2010) studied enhancing the drawing process with a closed chamber and an airflow towards the collector as [Figure 4].

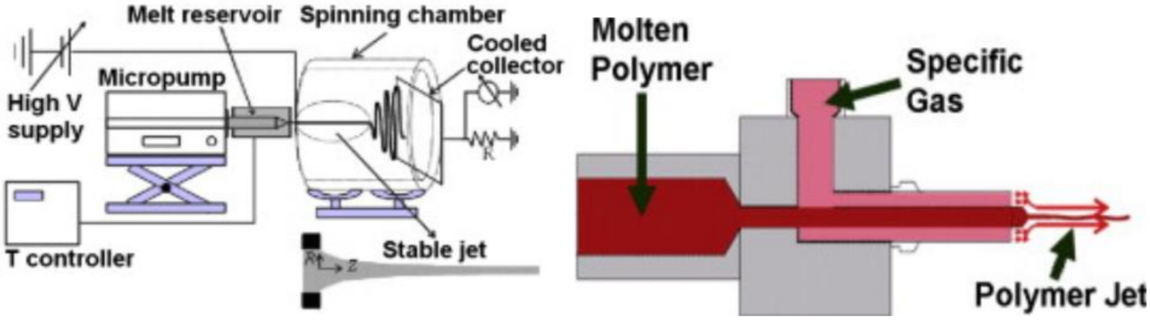

Figure 4. The figure of GAME (Gas Assisted Melt Electrospinning) system (Zhmayev et al. 2010).

The melt reservoir is heated to above the melt point of the material, Polylactic acid, and the nozzle is heated with another hot air stream with a temperature ranging from 40 to 150 °C. The gas is supposed to perform a precise temperature control near the nozzle area and providing some additional drawing force. However, in this study, it is hard to define which part is really contributing to the drawing process. Another problem is the complexity of the system. If there are multiple nozzle spinning simultaneously, providing multiple gas channel with identical temperature and air flow rate is a technical challenge.

Increasing the electric intensity is also a way to increase the drawing force. However, discharges will happen if the electric field intensity is too strong and the spark discharge is harmful to the fiber. The shock will break the Taylor cones and the continuous fiber jet. Discharges are not rare in electrospinning study, this kind of discharge could easily happen when the intensity is over 500 kV/m (Kaiser 2006) which is not a high enough electric intensity to produce ultrafine fibers from polymer melt. So, avoiding discharges is an important topic and not adding electrical part near the cone forming area is a possible solution. The study by Ogata et al (2007) introduced a creative way to heat the polymer remotely by CO_2 laser. This heating method is effective to avoid the discharge at the sharp needle or nozzle. The scheme for this work is shown as [Figure 5], the polymer source is a rod and the tip of the rod is irradiated with CO_2 laser from three directions where the solid polymer turning to melt. Between the polymer source tip and the drum collector, the voltage difference is 16-41 kV.

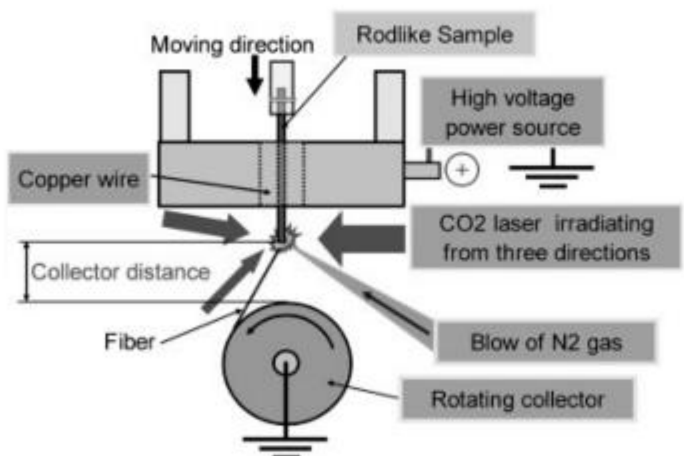

Figure 5. A scheme of the laser heated melt electrospinning system (Ogata et al. 2007).

The material for this study is polylactide acid and the fiber diameter obtained is less than 1 micron. The molecular weight was measured in the study and the number average molecular weight has dropped 80% when heated with a 15W laser. This might be the reason that such thin fiber could be produced.

Another important technology tree in this area is created by the Beijing University of Chemical Technology. That group has been working on a melt electrospinning with a funnel-shaped nozzle in [Figure 6] called Melt Differential Electrospinning. There are two concentric metal funnels in the end area. The space between the two funnels is serving as the nozzle and the inside area of the smaller funnel is the channel of air. The cross-section view of the nozzle looks like a ring that allowing multiple fibers to spin at the same time. The airflow from the center is helping the fiber attenuation.

The polymer melt will go through the following four steps (Li et al. 2014a): first, the melt was transformed from a cylindrical flow into a uniform ring-like flow, next, the ring-like flow was distributed to the umbellate nozzle, then a thin and uniform melt film formed on the umbellate circumferential surface, finally, when the applied high voltage surpassed a critical value, self-organized multiple jets around the rim of the umbellate nozzle were ejected to the receiver plate spontaneously.

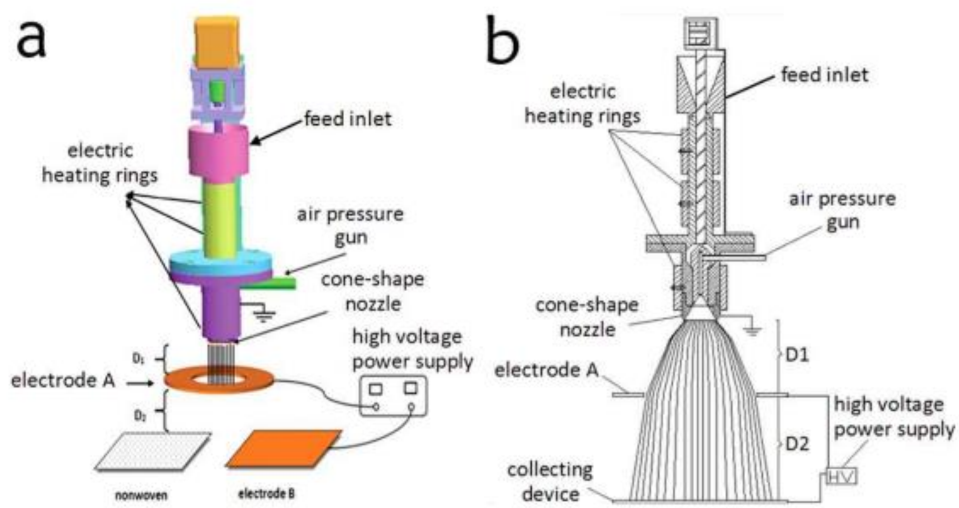

Figure 6. A scheme of the differentiate melt electrospinning system (Li et al. 2014b).

The ring has a diameter of 52 mm, the inter-jet distance is 2.8 mm and there could be more than 100 jets existing at the same time. When applying an air assist drawing system, the fiber diameter could be 5 μm on average.

As the movement of melt electrospinning is more controllable than the solution method, Farrugia et al. (2013) achieved the goal of directly writing by using a platter movable in 2D direction as the collector. The collector's movement is tuned with the spinning movement so the straight lines could be deposited. The fiber diameter ranged from 12.5 to 20 μm, and the material was PCL. As shown in [Figure 7], many orientations are successful at the speed of 1 m/s.

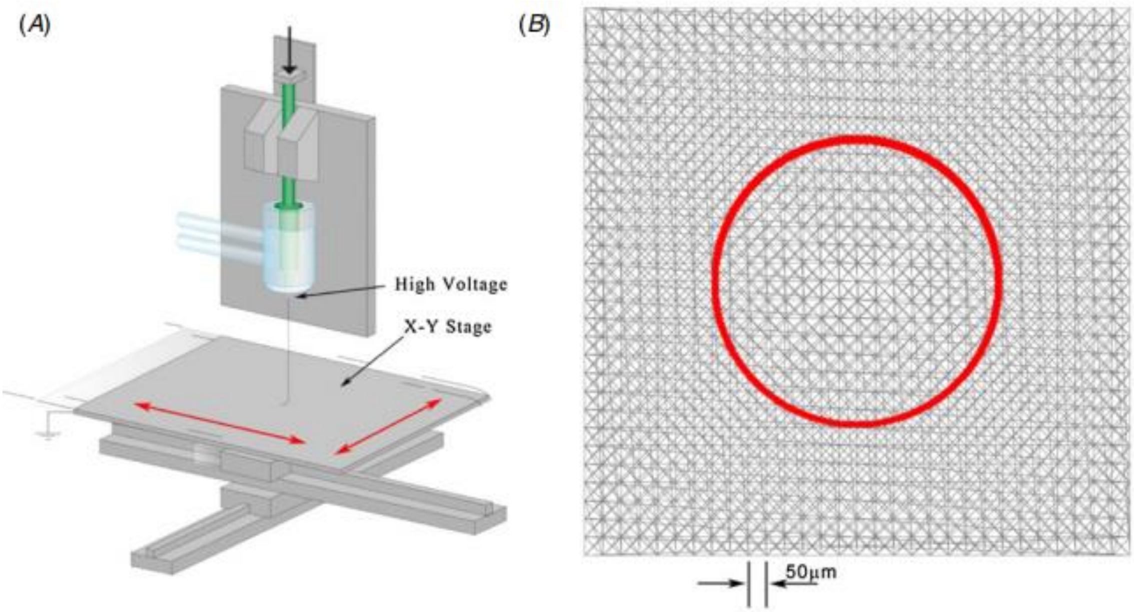

Figure 7. The schema of the direct writing melt electrospinning setup and the written patterns (Farrugia et al. 2013).

For the goal of getting smaller fibers and faster production rate, the modifications of melt electrospinning setups could be concluded in [Table 2],

Table 2. The comparison of exsisting process-focused melt electrospinning methods.

Method Name	Material	Fiber Diameter	Production Rate	Comments
Gas Assisted Melt Electrospinning	PLA	0.18 µm	single jet	An effective way of getting sub-micron fibers. The airflow effect is combined with electric force to attenuation.
Laser Heating	PLA	1 µm	single jet	molecular weight dropped significantly, weaker mechanical property.
Differential Melt Electrospinning	PP	12 µm	2.8mm/jet	Polymer fed by an extrusion system, airflow is also involved.

Those projects performed various creative ways of getting smaller fibers or increasing production rate. However, there is still lack of approach that can produce sub-micron fibers in a high throughput rate with a simple setup. The material for those study are PLA and PP, both are materials easier to produce thinner fibers. There are only a few melt electrospinning paper used polyethylene (Larrondo and St. John Manley 1981; Deng et al. 2009). The old paper could only produce fiber diameter at 138–190 µm. The later paper spun LDPE from a single-nozzle syringe setup producing fiber with 5-33 µm in diameter which is a great progress but still relatively thick than fibers in other material.

In order to study the principles of needleless melt electrospinning, also for producing ultrafine fibers without the effects of airflow and the extrusion movement of the polymer melt, Wang et al. (2014) conducted electrospinning at a flat aluminum plate edge. This work successfully spun the fiber without any feeding system, let the Taylor cone be created spontaneously, and discussed the relationship between polymer temperature with jet forming speed, jets number, and fiber diameter.

2. RESEARCH OBJECTIVE

This work is a continuous improvement of the work of Wang et al. (2014). When repeating the experiments of Wang's work, the variation in jet number and fiber diameter was huge. At some optima conditions, the fiber diameter could reach to 20 μm and about 15 jets spinning simultaneously. In the bad case, there could only be 7 jets and the fiber diameter could reach 100 μm. This study analyzed the causes of the variation and designed an optimized update of the old melt electrospinning system with a new configuration. This new system is focusing on control and enhances the intensity of the electric field near the Taylor cone initiating area. Supported by simulation result, the study concluded several possible instrument arrangements for the system and made systematic experiments to test the schemes. The final new design increased the intensity of spinning area by 10 times with the same voltage applied at the collector and the same spin edge to collector distance. and decreased the fiber diameter by 20% comparing to the original setup could produce.

Another aspect is that the optimization provided a more stable small environment that can provide more robust data against the possible change of the environmental parameter. It also discussed about environmental parameter's effects. Revealed how will the distance of spin area, voltage difference between the edge and the collector, polymer temperature, spinning area temperature affect the jets number, the yield rate, the fiber diameter and the morphology of fibers.

3. MATERIALS AND EXPERIMENT DETAILS

3.1. Materials and instruments

The material and instruments used are stated in the following table. All materials are used as purchased status. The [Table 3] shows the materials and instruments used in this work.

Table 3. Materials and instruments used in this study.

NAME	MAKE	MODEL
Poly(ethylene) PE	Dow	ASPUN 6850A
DC high voltage power supplier	Glassman High Voltage.	PS/FC60R02.0-11
Hot Plate	Barnstead International	SP131325
IR Heater	TempCo	Customized gold coated IR lamp 1000W
Ceramic heater	TempCo	Steel housing 1000W
Freezer Mill	SPEX CertiPrep	6750

3.2. Experiments

3.2.1. Preparation of PE powder

The polyethylene used in this work is ASPUN 6850A provided by DOW, in the form of pellets. This is a linear low-density polyethylene (LLDPE) with the melt temperature of 131 °C and the density of 0.955 g/m^3. The melt flow index of 30 g/10 min (ASTM D 1238 standard). The granule is too large for the precise study of spinning function. It is tested to have a rough surface of the molten polymer layer which is interrupting the foaming of Taylor Cones. On the other hand, due to the space between granules, there will be a considerable sum of bubbles in the polymer melt, which is going to increase the oxidizing rate and give more uncertainty to the morphology.

Subsequently, all polyethylene pellets used in this work are first ground with a freezer mill in the following steps.

1. Put the PE granules in the vial container of the grinder, fill the tank with liquid nitrogen (LN).
2. Close the lid, set the grinding time to 2 minutes, rest time to 1 min, work for 4 cycles at the rate of 8.
3. PE pellets will be ground into powder, the size is similar to commercial cooking salts.
4. Collect the ground powder in a sealed container for later use.

3.2.2. Procedure of electrospinning

Although there are many modifications, the principle of this unconfined melt electrospinning can be shown as [Figure 8] and [Table 2Table 6].

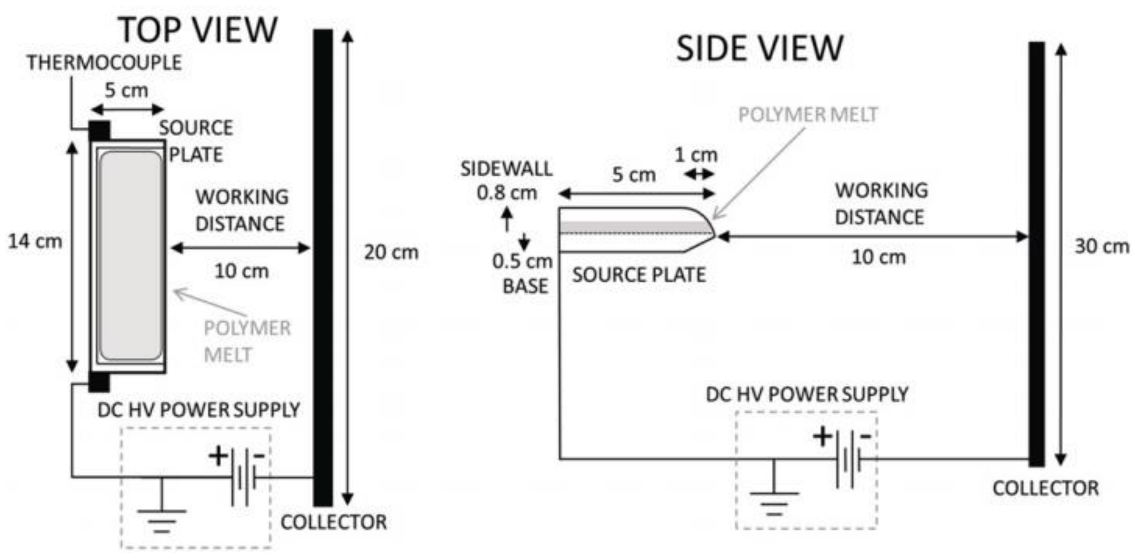

Figure 8. Schematic diagram of the setup (Wang et al. 2014).

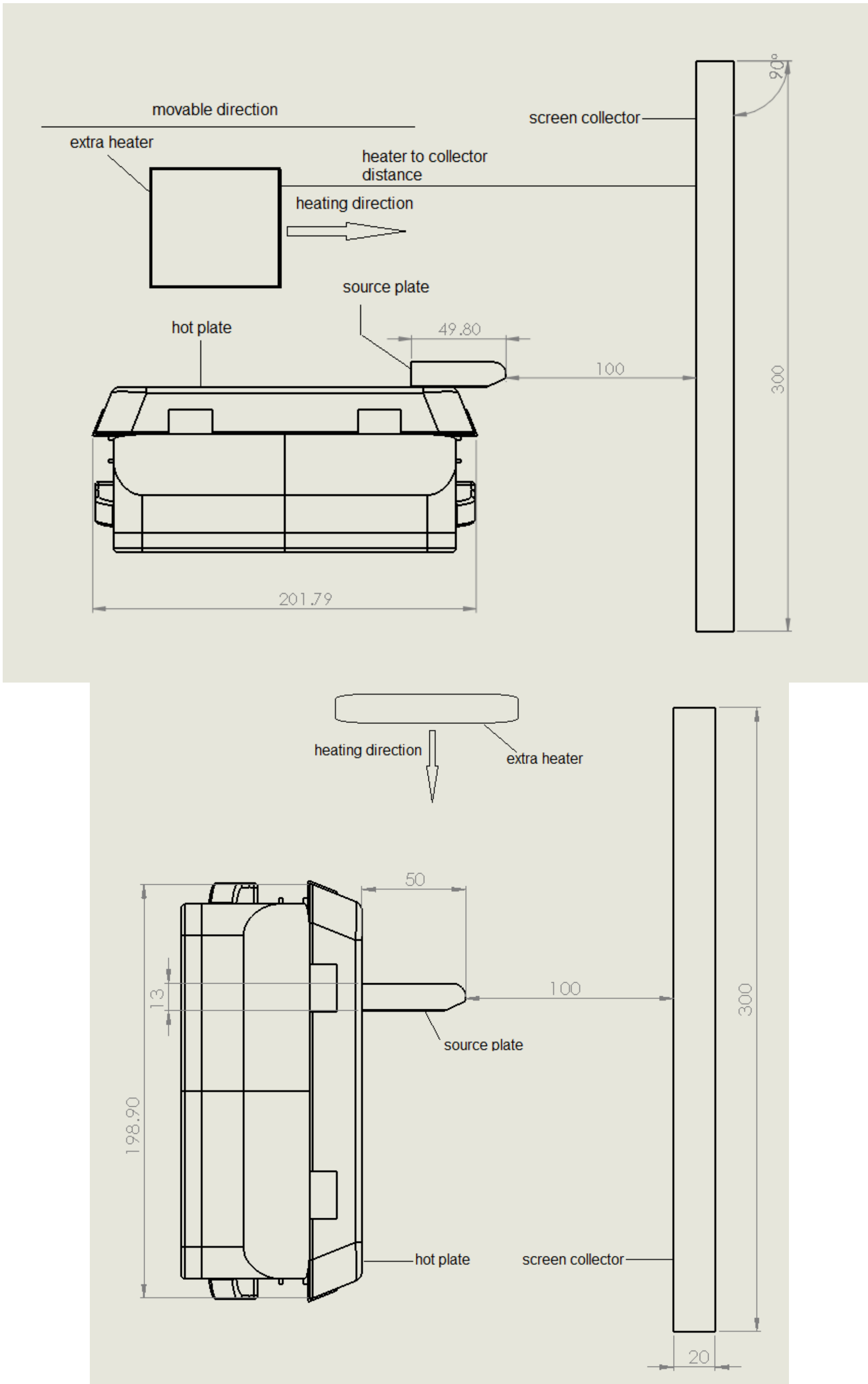

Figure 9. The scheme of horizontal and vertical configuration of the setup.

There are two main parts of the system, fiber generation part and the collecting part. The fiber generating part consists of heating sources and polymer source plate. The heating sources are a hot plate and two infrared heating lamps. They could either work together or separately.

The source plate is a customized aluminum plate. It has three short walls and one side unconfined where the fiber will come out from. The plate is placed with its short side facing the operator. There is a grounded cable connected at the far short wall and a K type thermocouple fixed between little ceramic tiles (15 x 14 x 5 mm) at the near wall of the plate.

There are several configurations of the setup. The hot plate could be placed underneath the source plate in the level state or standing vertically by its side surface. When putting the hot plate under the source plate, the spinning edge is protruded over the edge of the hot plate. In the second form, the source place will be fixed to an aluminum holder with its long wall. The holder is hanging against the vertical ceramic surface of the hot plate. Although there are several versions of the setup, the hot plate is always isolated from the table with a rubber mat or multiple layers of foam.

The collector is a 30 cm x 30 cm double-layer square board. The surface facing the source plate is made of stainless steel connected with negative polarized high voltage supply. An “L” shaped acrylonitrile butadiene styrene (ABS) plastic stand is holding the metal board from the back. To prevent electrical discharging at the edge of the steel board, they are covered by electrical tape. The collector is standing vertically and perpendicularly to the table. It is isolated with rubber mat as well.

The distance between the edge of the source plate and the collector metal surface is named working distance. The range of spinning distance for this work is from 8 cm to 14 cm.

The default procedure for this work is,

1. Turn on the heating source at a selected level, wait until the thermocouple placed at the near side of the source plate shows 190°C.
2. Place 10 g of ground polyethylene powder to the source plate evenly. Let the polymer powder preheated in the closed chamber until the thermocouple reached 190 °C again and make sure the polymer is thoroughly melted, showing transparent status.
3. Turn on the power supply, increase the voltage to the working voltage gently. The default voltage for this work is -45kV. This is also the start point of video recording by a camcorder (VIXIA HF R800, Canon). A LED light (Model 900410) is the assisting illumination source.
4. In the high electric field, the Taylor cone should generate at the edge of the molten polymer and a fiber will come out at the tip of the Taylor cone.
5. Wait until the selected time. 20 min is the default working time for this work. Turn off the power of high voltage and the heating source, then collect the products with a re-sealable zipper bag.

3.3.3. Quality assurance of experiments

When repeating the work of Wang et al. (2014), the fiber diameter varies in a wide range. Sometimes the average diameter is ~20 μm but sometimes it could reach 100 μm. To find out the error causing factor, a control variable investigation was conducted.

The investigation was conducted following the factors that affecting melt electrospinning in section 1.4.2.

Melt flow rate is determined by the nature of material. The material for this study is supposed to be the same material as Wang used before. The model of polyethylene has been checked and another bag of ASPUN 6850A was acquired from DOW. The results from new 6850A didn't show any difference with the old batches.

The molecular weight of the polymer is affecting the MFR as well, and the most likely factor that could change the molecular weight should be the heating time during the spinning. For this concern, the Standard Operation Procedure (SOP) is noted that the preheating process needs the attendance of operator to make sure to turn on the high voltage power immediately after the goal temperature has reached. Overheating is strictly forbidden in this study and the source polymer should be changed after each experiment. However, the quality improving exercise of the process didn't help.

Move to the second factor, the spinning voltage was calibrated by a high voltage probe (Fluke, 80k-40). The output of the high voltage supply is constant during 5 tests, so this should not be the affecting parameter.

The spinning distance was checked before every experiment with a 10 cm cardboard ruler. The source plate is usually put a little closer to the collector. It will be pushed back to 10 cm by the ruler to guarantee the accurate distance.

The last factor is the melt temperature. Although PE melt viscosity is not sensitive to the temperature in the range of 150 – 200 °C (W. L. Peticolas and J. M. Watkins 1957), several modifications were applied to make the temperature control become more accurate. The thermocouple fixed between the ceramic tiles on the source plate is covered with thermal paste (HALNZIYE, HY880) to enhance the thermal conductivity. To make sure the temperature of the plate is consistent with the polymer melt, the temperature reading is calibrated by inserting thermocouple directly into the PE melt. Although the temperature in the polymer melt is lower than the plate temperature, the temperature difference is always the same. After all the steps have applied to the process, the difference was still there.

Table 4. The debug process and measures taken in this study.

parameter	MFR (g/10 min)	voltage (kV)	distance (cm)	Polymer melt temperature (°C)
measures	Repeat experiment with new PE 6850A, no difference.	Calibrate the power supplier	Update SOP by pushing the working distance from 9.x cm to exact 10 cm every time.	Calibrate the thermocouple.
	Update SOP prevent overheating of the polymer melt.			Increase the conductivity of the temperature sensor.

3.3. Characterization

3.3.1. Sample preparation

The fiber spun at the collector distributing in a roughly 10 cm x 5 cm area in [Figure 10].

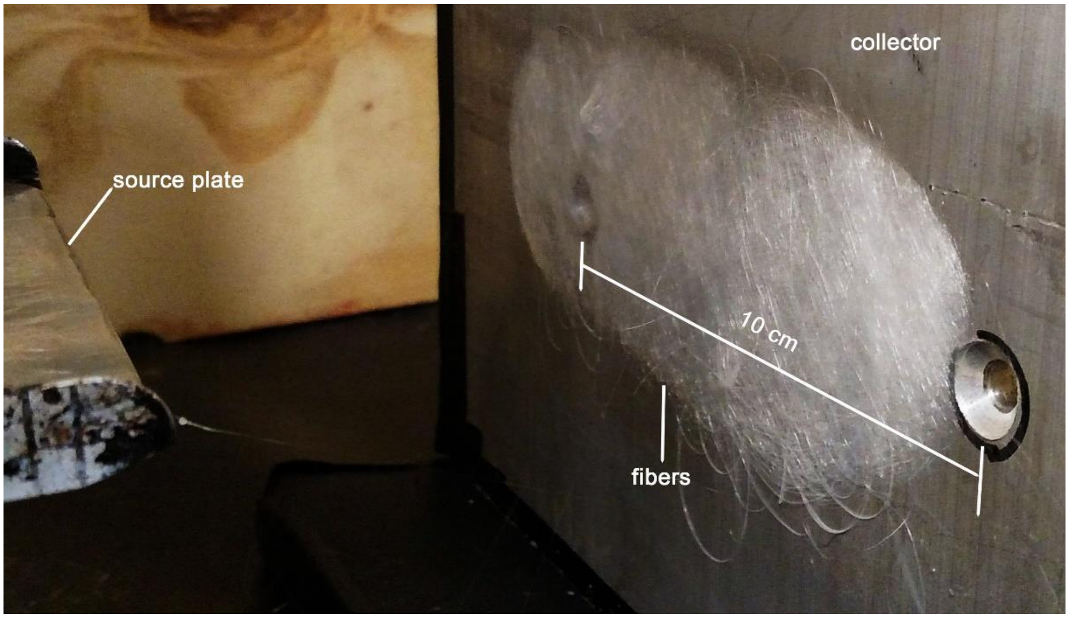

Figure 10. The photo of fiber distribution at the collector

Fibers are held on the collector with static electricity force and could be picked up easily from the collector. After been picked up, the hole ball of fibers will be disorganized by rubbing and kept in zip-loc plastic bags.

Before taking photos by microscope, the sample will be carefully observed and the most condensed area with be cut off from the ball. Usually the cut sample is like a piece of fabric instead of a bunch of loose fibers if the diameter is less than 50 μm. [Figure 11] shows the area to be cut. The piece of fiber is dispersed into a layer and placed on containing board for microscope imaging. The sample for SEM imaging is shown in [Figure 12].

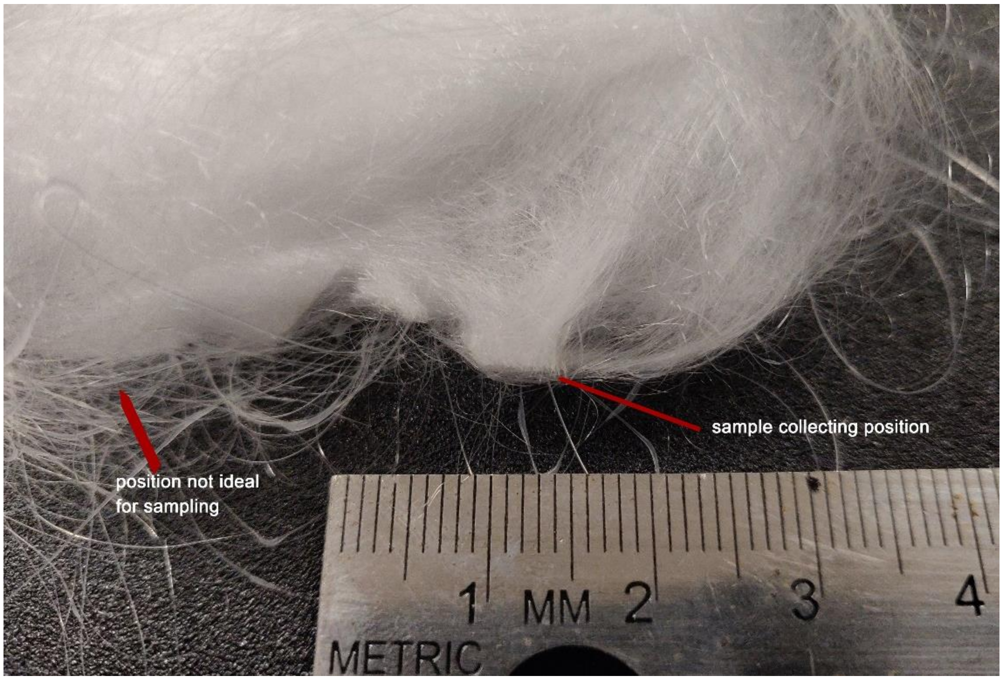

Figure 11. The area to be chosen for fiber diamerter measuring.

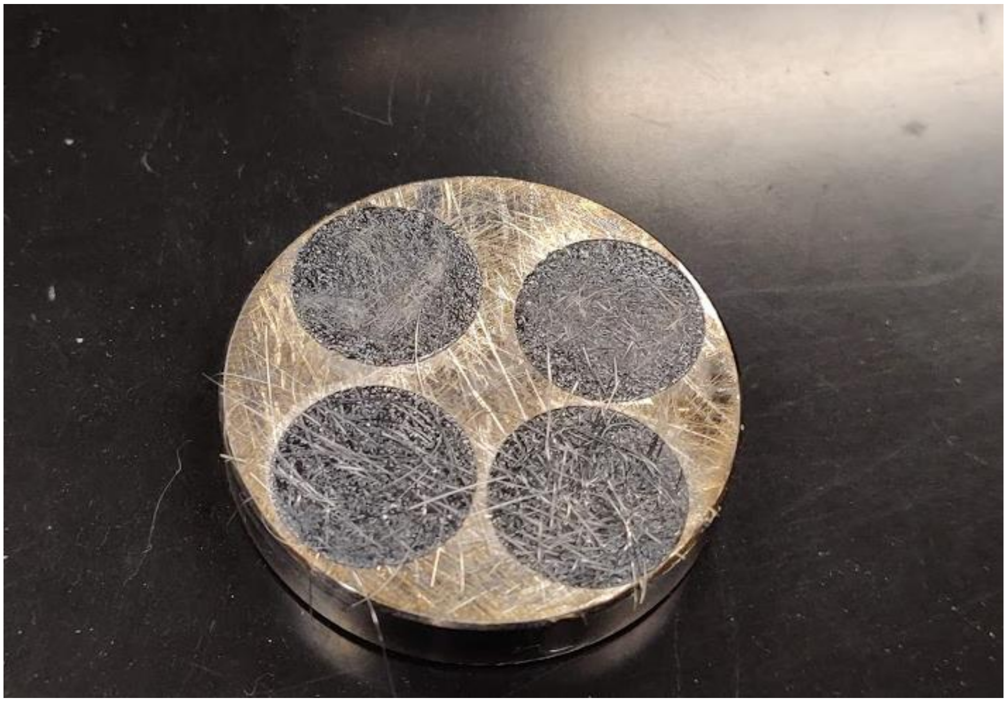

Figure 12.The sample for SEM imaging.

In this study, only one sample is taken for one experiment and 3 to 4 experiments are repeated at a same condition.

3.3.1. Optical microscopy

To determine the diameter and the shape of the fibers, a microscope (LV100N, Nikon) is used to take photos. If the fiber sample is visually characterized as thick fibers (larger than 50 μm), it will be observed by optical microscopy. The sample is placed in oil between a microscope slide and coverslip to increase the visibility. Samples are observed by a 100x lens. Every sample are checked with a wide range of zooms in case there are some ultra-huge or ultra-small fibers missing by unfocused.

3.3.2. Scanning electron microscopy (SEM)

If the fiber is very small (smaller than 50 μm) and entangled together like a membrane, it is categorized as small fibers and observed by SEM. Small fiber samples collected directly from the collector are cut into small piece and spread into a thin layer on the top of the carbon tape. They are sputter coated with Au-Pd at a thickness of ~10 nm (Quoron Technologies, S67620). Two SEM instruments are used for this work, a Variable Pressure SEM (Hitachi, S3200N) at AIF, North Carolina State University (NCSU) and a Phenom FEI desktop SEM at College of Textiles, NCSU.

The accelerate voltage is usually 35kV and the image are taken at the magnification between 1000 to 3000 times.

After each observation, the measurement of fiber diameter is measured with ImageJ software (Ver.1.52a). Set the scale based on the scale bar of optical microscopy or SEM photos at first, then the software can transfer the pixels length on the screen into real length automatically. The basic rule of the measurement is measuring each fiber only once and have more than 50 fibers for each sample.

3.4. Finite element analysis of the electric field

The simulation is conducted with ANSYS Electronics Desktop (Ver. 19.1). The model is built with Solidworks (2016 Ver.SP04) precisely and imported into Electronics Desktop. The simulation area is a 600 mm cubic area [Figure 13]. The purple area in [Figure 13] touching the spinning edge of the source plate is the focused area to plot the electric field.

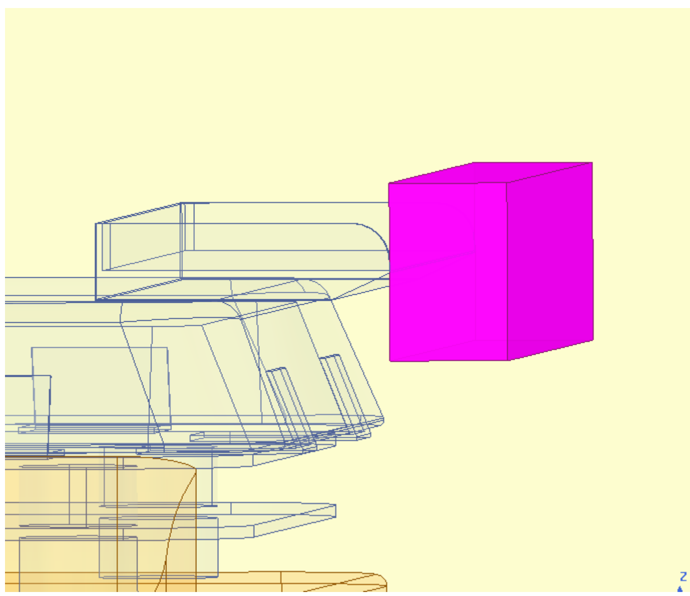

Figure 13. The 3D model of the simulation focus area.

The maximum mesh length is 1 mm and there could be as much as 100,000 meshes in one simulation.

The materials are assigned to the closest material in the build-in database and the voltage excitations are noted, including the grounded areas.

3.5. Statistical analysis

The fiber diameter is measured by ImageJ, using more than 50 data for each sample. The data is summarized in JMP pro (SAS, Ver. 13), and conducted one way analysis of variance (ANOVA) when comparing the dependent data as the function of different parameters in the same category. $P < 0.05$ is a significant difference and $P < 0.01$ is a very significant difference.

4. RESULTS AND DISCUSSION

[Figure 14] is the roadmap of this study. Experiments were conducted according to this logical sequence.

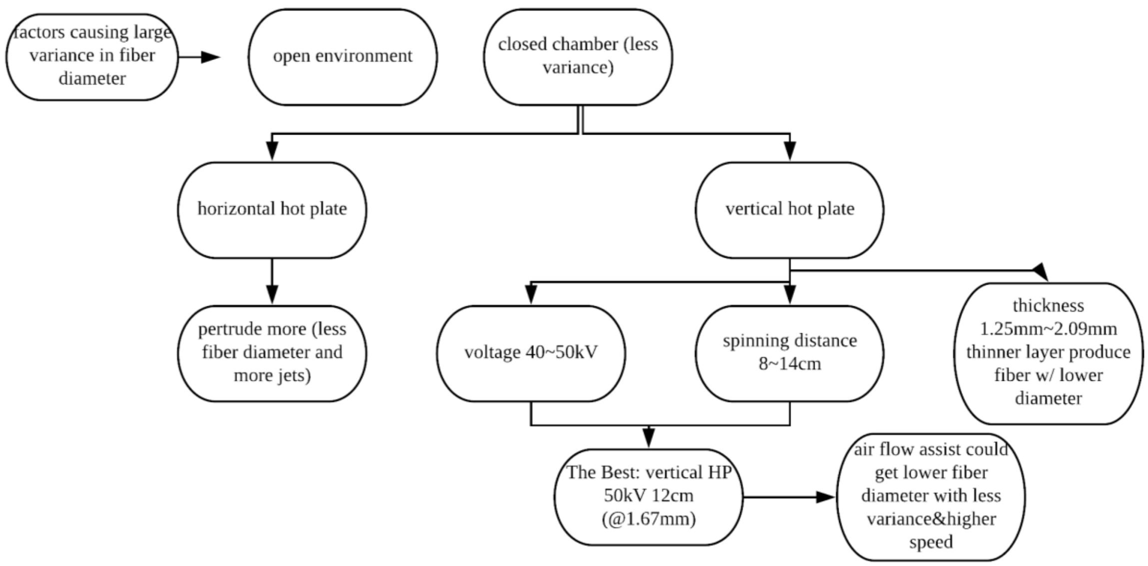

Figure 14. The roadmap of this study.

However, the discussion part is organized base on the importance of factors which is setup configuration, voltage, and working distance, ambient temperature, air flow in the system. As polymer melt layer thickness study was in a different setup configuration to other experiments, it is discussed separately at the end.

4.1. The configuration of the setup

During reviewing videos, a phenomenon has been identified that the protruding distance of the source plate by the underneath heater is affecting the process significantly. [Figure 15] shows the side view of the relative position of the source plate and the hot plate:

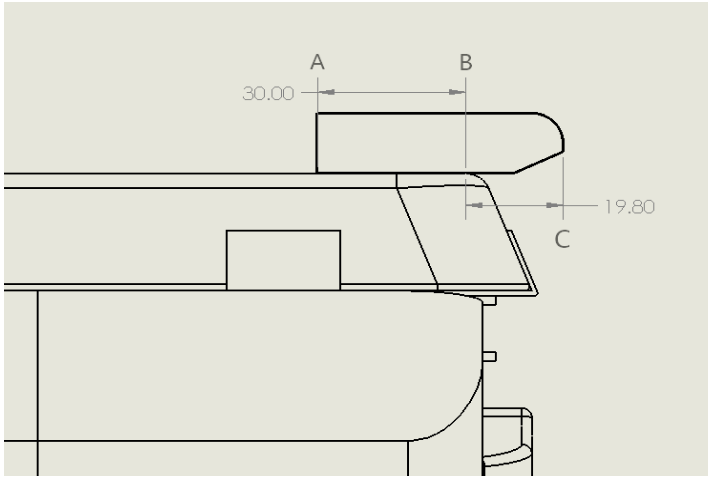

Figure 15. The side view of the source plate and the hot plate underneath.

The protruding distance is BC, which is the distance from the edge of the plate to the tangency contact point of the source plate. However, it is hard to measure because of the chamfer angle of the hot plate. Thus, AB is introduced to determine the position of the source plate alternatively in this work. AB, as it is shown in [Figure 15], is the distance between the end edge of the source plate and the tangency point of the hot plate. Here, the AB is named the contact distance and the protruding distance is calculated by using plate width subtracting the BC. [Figure 16] is describing the trend that how the jets number is affected by the protruding distance (BC).

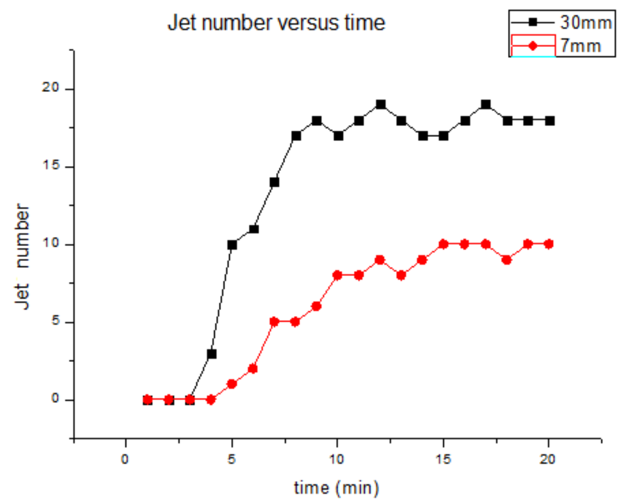

Figure 16. The jets number along with the experiment when the source plate is protruded 7 mm and 30 mm.

In one observation of the spinning at 10 cm working distance, 45 kV voltage condition (45 kV is the voltage difference from the source plate to the collector, the actual situation is that the source plate is grounded at 0 V and the collector is charged at -45 kV. The following contents use the same expression), when the protruding distance is 30 mm, the Taylor cones initiated faster than the scenario that the plate protruding only 7 mm. After the process became stable, the plateau area in the plot, after 10 min, the plate with longer protruding distance has about twice jets as the shorter one. Fiber diameters are different as well. The average diameter of fibers spun with 30 mm protrude distance are 13 ± 3 μm while the sample produced with 7 mm protruding distance are 70 ± 4 μm. The fiber diameter was test by one-way analysis of variance (ANOVA) and the results is in [Figure 17].

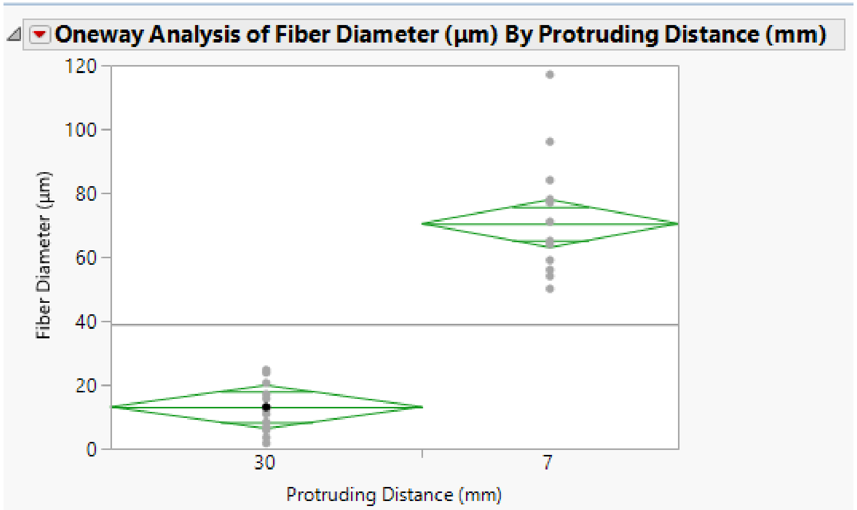

Oneway Anova

Summary of Fit

t Test

7-30

Assuming equal variances

Difference	57.3406	t Ratio	11.63108
Std Err Dif	4.9299	DF	29
Upper CL Dif	67.4234	Prob > |t|	<.0001*
Lower CL Dif	47.2577	Prob > t	<.0001*
Confidence	0.95	Prob < t	1.0000

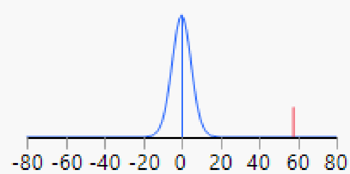

Analysis of Variance

Source	DF	Sum of Squares	Mean Square	F Ratio	Prob > F
Protruding Distance (mm)	1	25242.903	25242.9	135.2820	<.0001*
Error	29	5411.247	186.6		
C. Total	30	30654.150			

Means for Oneway Anova

Level	Number	Mean	Std Error	Lower 95%	Upper 95%
30	17	13.0880	3.3130	6.312	19.864
7	14	70.4286	3.6508	62.962	77.895

Figure 17. ANOVA results of fiber diameter by setup protruding 30 mm and 7 mm.

The difference is very significant that the P-value is < 0.0001.

This discovery indicates that the general model of the electrical field strength:

$$E = U/l$$

where E is the electric intensity, U is the voltage difference and l is the distance

This formula is not suitable to analyze this question in the micro view.

To discuss this question in detail, the basic idea is that the distribution of electric intensity is based on the position of certain electric potential points. In this question, the determination points are the shape of both electrodes, the grounded source plate and the negatively charged collector.

To analyze the micro view electrical field, it's better to understand how the electric field at every point in the system is. As the relationship between electric intensity (E) and the electric potential (φ) is,

$$E = -\nabla\varphi$$

the position that the electric potential drops faster will have a more condensed electric field. It is not hard to understand that the electrical potential dropping in this system is uneven because the shape of both electrodes are not parallel plates. The whole source plate and the grounded hot plate are at equal electric potential and there should be all the electric field lines from the 0 V potential surface to the -45kV collector. As the shape changes so suddenly near the edge, the electric potentials are changing at different pace in that condensed area. As a result, the electric field intensity should be uneven as well and it should be stronger near the sharp edge.

To quantify the electric intensity, we need to know intensity at a point in the field is:

$$E(x,y,z) = \frac{\boldsymbol{F}}{q_1}$$

Where $\boldsymbol{F}$ is the electric force and q_1 is the unit positive charge.

Assume there is a point charge at the position of ***r'***, to calculate the electric intensity value at the position p (position vector ***r***), the formula can be expanded to:

$$E_p(\boldsymbol{r}) = \frac{q}{4\pi\varepsilon_0|\boldsymbol{r} - r^{'}|^2}\frac{\boldsymbol{r} - \boldsymbol{r}^{'}}{|\boldsymbol{r} - \boldsymbol{r}^{'}|}$$

Where ε_0 is the specific inductive capacity of vacuum.

However, that is just for the electric field induced by a single electron. What if there are a group of electrons? The electric intensity should be integrated into:

$$E = \frac{1}{4\pi\varepsilon_0}\sum_{k=1}^{n}\frac{q_k(\boldsymbol{r} + \boldsymbol{r}_k^{'})}{|\boldsymbol{r} - \boldsymbol{r}_{\boldsymbol{k}}'|^3}$$

For a surface that is:

$$E = \frac{1}{4\pi\varepsilon_0}\int_{S'}\frac{\sigma d\boldsymbol{S}'}{R^2}\boldsymbol{e_R}$$

S' is the analyzing area, R is the distance between the position and the origin, $\boldsymbol{e_R}$ is the unit vector describing the direction.

Based on the fundamental knowledge above, it is possible to get the specific electric intensity at some certain positions in the field. This integral calculation could be processed by the finite element simulation software, ANSYS Electronic Desktop (Ver. 19.1) based on the 3D model of the system. The model is built with Solidworks (Ver. SP04). Considering the edge effects, all edges have been trimmed with round fillets.

The steps have been stated before. The focus area is a narrow rectangle perpendicular to the source plate spinning edge. The size is 140 mm (L) x 2 mm (W). The data is provided at every 0.5 mm. The color plot of electric intensity is shown as [Figure 18]. The left one is the simulation when the source plate protruding 10 mm of the hot plate while the right source plate is protruding 30 mm.

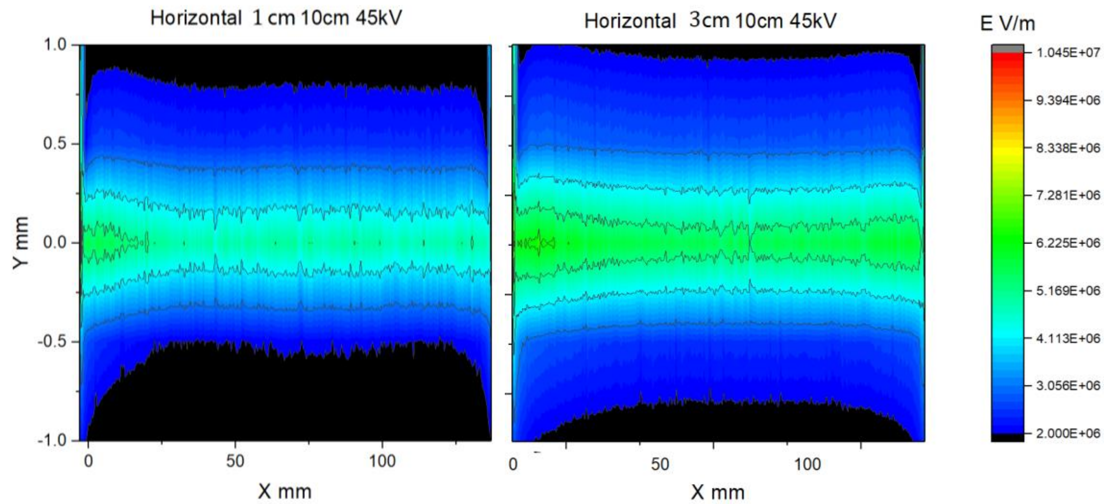

Figure 18. The electrical intensity map at the edge of the source plate.

The color scale is set to start from the cold blue at 2 x 10^6 V/m to the warm red at 10.45 x 10^6 V/m. The area with the electric field below 2 x 10^6 V/m is shown in black as a result. The plot shows that at the same spinning distance and voltage, the source plate protruding more has a stronger electric field. This is enhancing the spinning process.

However, the gravity center of this 48 mm wide plate is calculated to be 26.88 mm away from the spinning edge by Solidworks. This length means that the plate could only protrude the hot plate no more than 26.88 mm without extra holder otherwise it will drop off from the surface of the hot plate. To maximize the electric field intensity, changing the configuration is necessary.

The heating source has been an annoying problem for many researchers (Ogata et al. 2007; Li et al. 2014b). Though not for the reason that they want more exposure area for the polymer source, the heating source is usually conflicting with the high voltage and this is the reason that Ogata et al. used a laser heating source in their study. However, the laser heating source is expensive and complicated. A non-contact heating source could be replaced by hot air as well but the heat gun with that high power usually has a too strong air flow for ultrafine fibers. It is working to some extent but not suitable for the study of jet forming project, so hot air is not applied as the heating source in this study.

Another common non-contact heating is the infrared (IR) heating. On the contrary to the laser, IR generated by normal heater is not focused and has worse directing ability. An IR lamp is suitable for heating the whole area instead of a specific position, so the addition of an IR heater is changing the whole spin line temperature.

As contact heating still has its value in this study, according to the idea to make the most exposure for the spinning edge, the configuration of letting the hot plate heating from the back has been designed. A 140 mm x 40 mm aluminum board is attached to the long wall of the source plate. Then, the assembly is bonded to the center of the hot plate's top surface. The scheme is shown in [Figure 19].

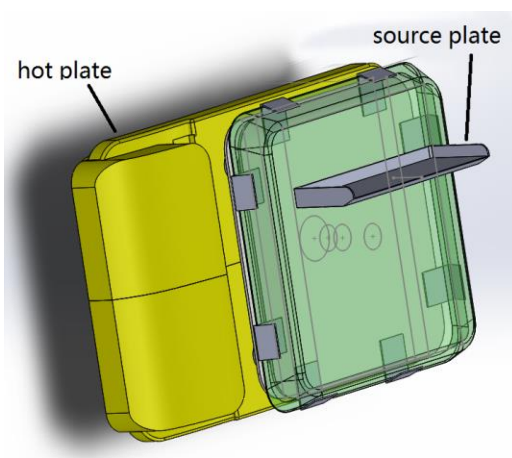

Figure 19. The 3D model of the vertical configuration of the fiber generation part.

As expected, the electric field simulation for this configuration shows even a greater intensity near the spinning edge than the “practically impossible” 3 cm protruding configuration. The comparison plot is shown in [Figure 20].

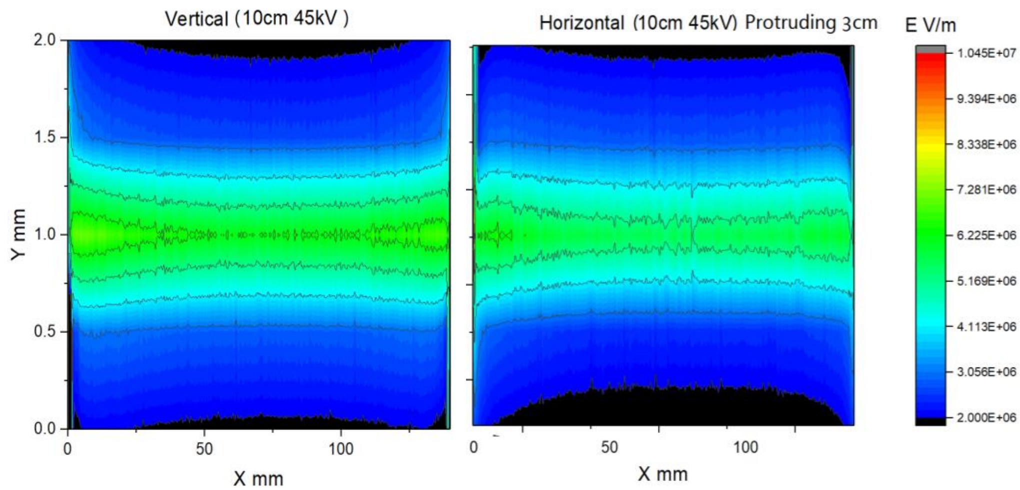

Figure 20. The comparison between the vertical and horizontal configurations.

The left plot, electric intensity color map for the vertical configuration, shows wider green area (strong electric intensity) and less black area (E weaker than 2 x 10^6 V/m) than the right one which is the “practically impossible” 3 cm protruding configuration. The ANOVA result for the electric intensity is in [Figure 21]. The 95% confidence interval of the electric intensity for horizontal 3mm protruding configuration is (2.9 x 10^6, 3.1 x 10^6) which is not overlap with the E of vertical configuration (3.1 x 10^6, 3.3 x 10^6). The P-value = 0.0003, indicating that the electric fields are very significant different. Thus, we can make the statement that the vertical configuration has a stronger electric field than the 3cm protruding horizontal situation.

Oneway Analysis of Column 2 By Column 1

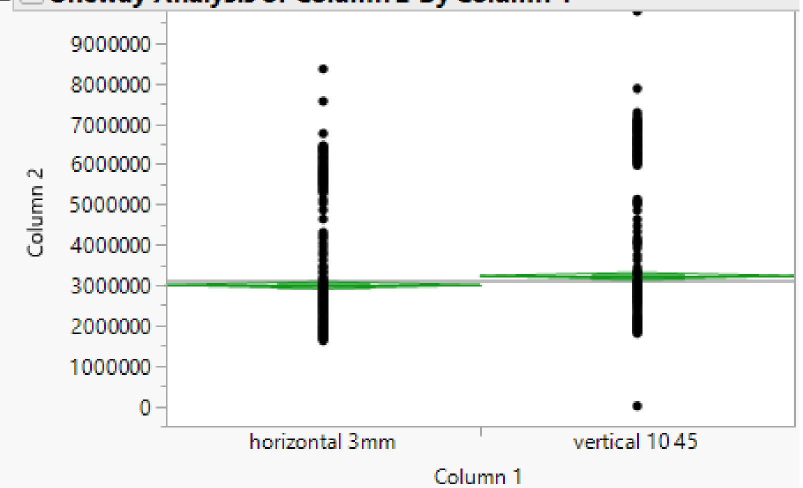

Oneway Anova

Summary of Fit

t Test

vertical 10 45-horizontal 3mm

Assuming equal variances

Difference	221039	t Ratio	3.657341
Std Err Dif	60437	DF	2808
Upper CL Dif	339545	Prob > |t|	0.0003*
Lower CL Dif	102533	Prob > t	0.0001*
Confidence	0.95	Prob < t	0.9999

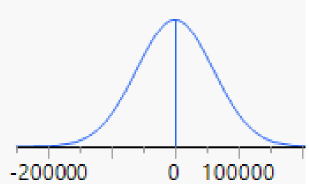

Analysis of Variance

Source	DF	Sum of Squares	Mean Square	F Ratio	Prob > F
Column 1	1	3.4323e+13	3.432e+13	13.3761	0.0003*
Error	2808	7.2053e+15	2.566e+12		
C. Total	2809	7.2396e+15			

Means for Oneway Anova

Level	Number	Mean	Std Error	Lower 95%	Upper 95%
horizontal 3mm	1405	3002249	42735	2918453	3086045.3
vertical 10 45	1405	3223288	42735	3139492.1	3307084.4

Figure 21. Average electric field intensity comparison for the vertical and the horizontal configurations.

However, due to the unfeasible of protruding the source plate by 3 cm in practical, the comparison experiments are conducted when the source plate was protruding only 1cm. The diameter difference and the jet number during the entire spinning process is shown in [Figure 22].

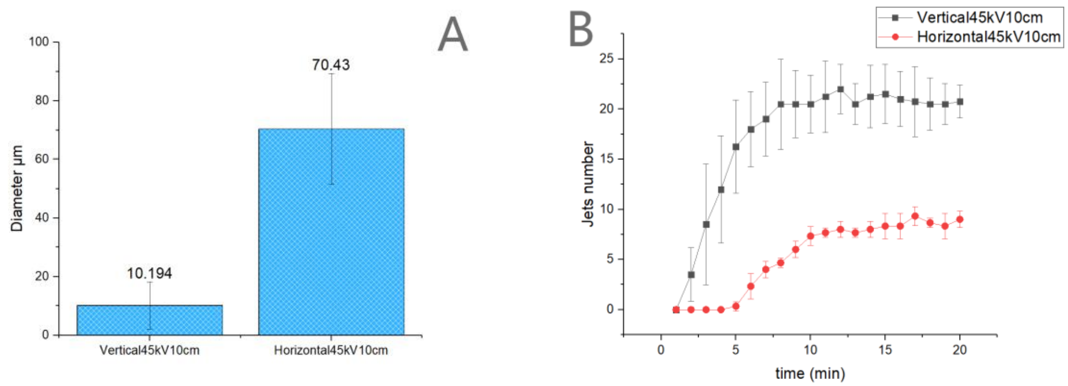

Figure 22. The comparison of the spinning process: A: average fiber diameter for vertical and horizontal configurations, B: Jet number as a function of spinning time for vertical and horizontal configurations.

The result shows that the vertical configuration perform better not only in fiber quality (85.5% lower fiber diameter) but also the spinning rate (298% more fiber jets simultaneously). The improvement of the fiber diameter is huge that the ANOVA shows that the P-value is less than 0.0001 and the 95% confidence ranges are not overlapped at all.

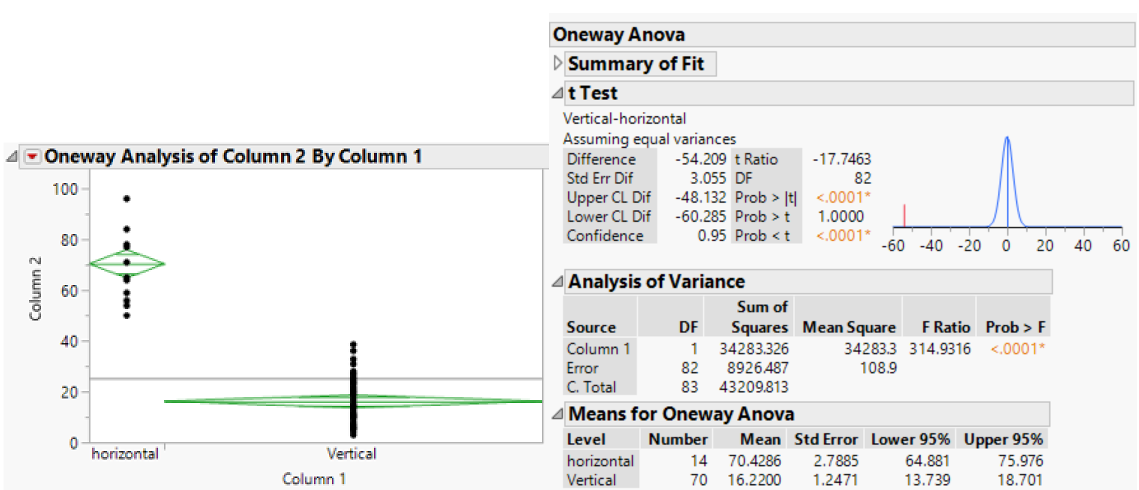

Figure 23. ANOVA of fiber diameter for vertical and horizontal configurations.

The vertical configuration also provided a warmer ambient temperature for the spin line.

Table 5. The spin line temperature for vertical and horizontal configurations.

Configuration	Temperature at 1 cm away from the source plate (°C)	Temperature at 5 cm away from the source plate (°C)
Vertical	50	43
Horizontal	43	30

Due to the restriction of setup, the data was obtained when the door of chamber was open. The real temperature in the closed chamber system was higher than the data above. However, the data set is still good to show the relationship that the vertical configuration has a higher ambient temperature than the horizontal one.

In conclusion, the thinner fiber and more jets performance are contributed by the cross function of the stronger electrical intensity and the warmer ambient temperature of the horizontal configuration.

4.2. Spinning voltage

After the ideal configuration that putting the hot plate vertically is set, other variables that might affect the spinning process could be discussed. The voltage has been discussed a lot in the previous researches of electrospinning and the proper distance is determine whether is able to spin or not. Thus, voltage effect to the spinning process should be discussed early. In this study, a series of the experiment about voltage was conducted, and the result is shown in [Table 6].

Table 6. The fiber diameter and stable jets number for vertical setup, 10 cm spinning distance.

Voltage (kV)	Spinning distance (cm)	Diameter (μm)	STD	Jets number	Jet speed (m/min)
40	12	N/A		2 after 15 min	
45	12	19	8	12	118
50	12	9	7	20	165
55	12	N/A		too many discharges	

As the literature (Kaiser 2006) presented, burst discharging usually happens when the electric field intensity is greater than 500 kV/m. It was proved in this study that the discharge happened a lot when the voltage was 50 kV and the distance was 10 cm. The spinning distance has been enlarged to 12 cm to assurance the successful of experiments at different voltages.

The spinning voltage range for this setup is not very broad. At the voltage of 40 kV, the electric field is too weak for the spinning process. After 10 min, 2 jets initiated and didn't increase until 15 min. 45 kV and 50 kV are proper to spin. 55 kV is too high for this configuration because discharge happened again.

The fiber spun at 45 kV has a significant larger diameter 50 kV when the spin distance was 10 cm. P-value for the ANOVA of fiber diameter = 0.0001.

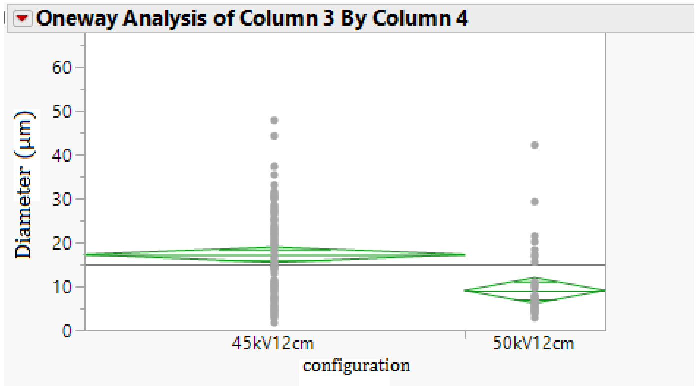

Oneway Anova

Summary of Fit

t Test

50kV12cm-45kV12cm

Assuming equal variances

Difference	-8.170	t Ratio	-4.72598
Std Err Dif	1.729	DF	183
Upper CL Dif	-4.759	Prob > |t|	<.0001*
Lower CL Dif	-11.581	Prob > t	1.0000
Confidence	0.95	Prob < t	<.0001*

Analysis of Variance

Source	DF	Sum of Squares	Mean Square	F Ratio	Prob > F
Column 4	1	2435.605	2435.61	22.3349	<.0001*
Error	183	19956.003	109.05		
C. Total	184	22391.608			

Means for Oneway Anova

Level	Number	Mean	Std Error	Lower 95%	Upper 95%
45kV12cm	135	17.2381	0.8988	15.465	19.011
50kV12cm	50	9.0678	1.4768	6.154	11.982

Figure 24. ANOVA for fiber diameter 45 or 50 kV, 12 cm.

The jets number of 50 kV is about the twice of 45 kV. The [Figure 25] helps to describe the trend.

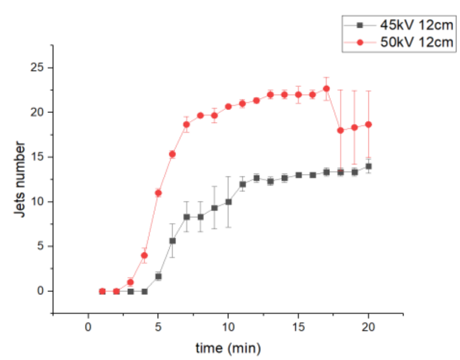

Figure 25. Number of jets during the 20 min spinning process when the voltage is 45 kV or 50 kV, distance of 12 cm.

Having more jets usually means more throughput, especially for the speed of throughput. The jet speed calculation is based on the total fiber throughput, average diameter, average jets number per minute and the density of the PE 6850A.

The volume per minute is:

$$\mathrm{V} = \frac{\overline{m}}{\overline{n}}/\rho$$

Where m is the mass of throughput, n is the jets number, ρ is the density of 6850A PE (0.955 g/cm^3). The speed per min (v) could be calculated with

$$\mathrm{v} = \mathrm{V}/\mathrm{S}$$

Where S is the cross-section area calculated base the average diameter.

At 50 kV, the jet speed is 164 m/min which is 39% higher than the 45 kV condition. The results indicate that a stronger voltage is still desired for higher production rate.

4.3. Working distance

The distance is another decisive factor that affecting the electric field intensity. By changing the distance at 45 kV working voltage, we observed the following results in [

Table 7].

Table 7. The spinning condition with various working distance, at 45 kV and 50 kV.

voltage (kV)	spinning distance (cm)	Diameter (μm)	STD	Jets number	Jet speed (m/min)
45	8	N/A		Too many discharges	
45	10	10	8	12	154
45	12	13	8	20	118
45	14	N/A		Hard to start	
50	12	9	7	20	164

The proper spinning distance range is still limited. At 8 cm, 45 kV, the system was not stable because spinning process was interrupted by discharging frequently. At 14 cm, the waiting time for the first jet is 12 min, and the jet got solidified and died after less than 2 minutes. They are either two short or too long for the process.

The jet number plot is [Figure 26]. The 10 cm condition has about twice jets as the 12 cm condition. The spinning speed is reduced due to the weaker electric field as well.

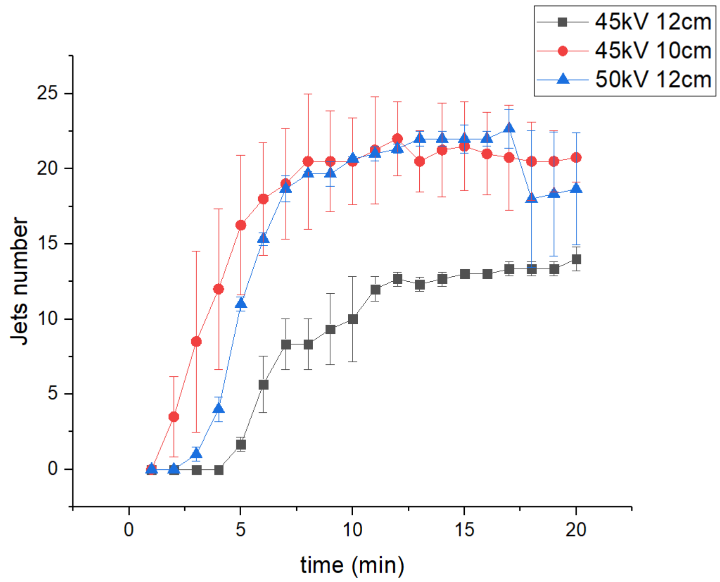

Figure 26. Jet number comparison at 45 kV with different working distance.

The 45 kV 10 cm curve is similar to the curve of 50 kV 12 cm. They are almost overlapped during the whole process. The fiber diameters are not statistically different as well. To quantify the effect, a simulation of the jet forming area was calculated and the plot shows in [Figure 27].

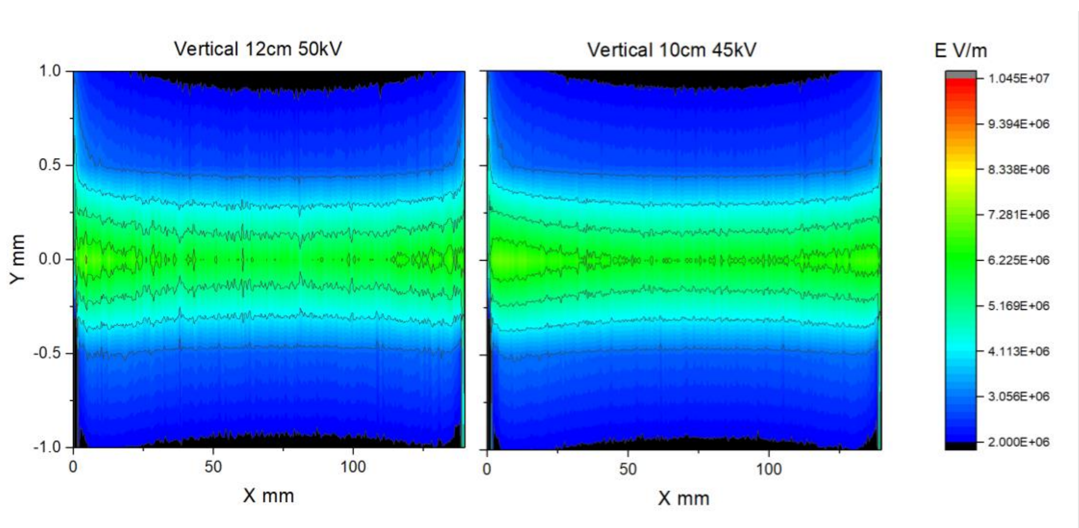

Figure 27. Color map of jet forming area for 12 cm 50 kV and 10cm 45 kV conditions.

The color map, especially the areas below 2 x 10^6 (black color) are close. The average E of these two conditions are 3.18 x 10^6 and 3.22 x 10^6 kV. In the whole simulation area, the Pearson Correlation Index of these two results is 0.9976 which indicates that those two electric fields are highly correlated.

This result is a strong support for the accuracy of the setup computing model and the calculation methods.

The difference of fiber diameter is not very significant for the spun condition at 45 kV 10 cm and 45 kV 12 cm. The P-value is a little larger than 0.05. However, the plot [Figure 28] indicates that the 10 cm shorter working distance is helping to have a narrower diameter distribution.

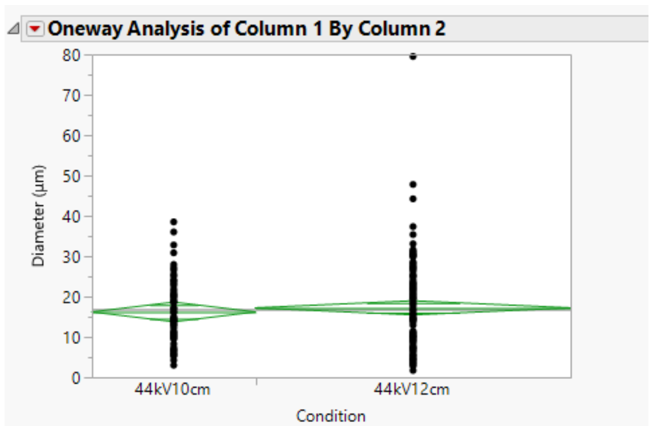

Oneway Anova

Summary of Fit

t Test

44kV12cm-44kV10cm

Assuming equal variances

Difference	1.0181	t Ratio	0.67009
Std Err Dif	1.5194	DF	203
Upper CL Dif	4.0138	Prob > |t|	0.5036
Lower CL Dif	-1.9776	Prob > t	0.2518
Confidence	0.95	Prob < t	0.7482

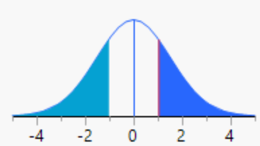

Analysis of Variance

Source	DF	Sum of Squares	Mean Square	F Ratio	Prob > F
Column 2	1	47.782	47.782	0.4490	0.5036
Error	203	21601.890	106.413		
C. Total	204	21649.672			

Figure 28. ANOVA of fiber diameters for 44 kV 10 cm & 12cm.

In conclusion, within the feasible working distance, the fiber diameter didn’t change significantly as the function of working distance. This is different from solution electrospinning that the fiber diameter decreases at first when the working distance increasing from a very small distance because the drawing distance is changing from too short to the sufficient distance. In this study, the drawing distance is always long enough allowing the full function of electric drawing force. The increase of distance is only resulting a weaker electric force and causing the increase of fiber diameter, though in a minor level. However, the decrease of jet speed is a bad effect of increasing working distance.

4.4. Ambient temperature

Melt electrospinning, as a spinning method derived from the melt spinning, has a lot of common parameters should be taken into consideration as the melt spinning and the ambient temperature of the drawing process should be discussed for quality assurance as well.

To study the influence of the spin line temperature, an extra heater (TempCo, ceramic IR 1000 W) was placed behind the source plate [Figure 29].

Figure 29. The photo of the setup with an extra ceramic heater.

Experiments conducted when the heater was at 28 cm, 21.5 cm and 15 cm away from the collector. The heater was equipped with a self-build PLC temperature controller with proportional–integral–derivative (PID) control and a Type K thermocouple. The temperature is set to 150 °C but the sensor at 3 cm away from the heater surface has never reached the set temperature so the heater was running at its max power constantly. The hot plate was placed at the horizontal direction and the power output is tuned with the extra heater to let the source plate temperature stick at 190 °C, wherever the position of the extra heater. The result shows in [Table 8] and the trends are plotted in [Figure 30].

Table 8. The fiber diameter change when an extra heater applied in the system.

Distance to collector (cm)	Temperature at 1cm (°C)	Temperature at mid-point 5cm (°C)	fiber diameter (μm)	STD
No heater	26	22	70	19
15	70	60	43	32
21.5	50	43	50	22
28	37	30	36	21

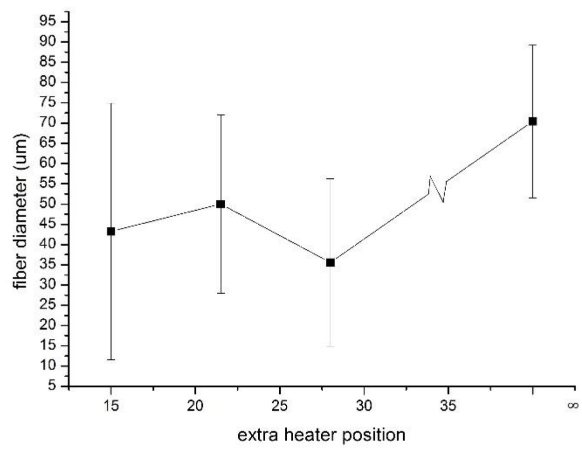

Figure 30. The trend of fiber diameter change when an extra heater applied in the system.

The plot shows a significant difference in fiber diameter before and after the extra is applied. However, fiber diameters are not so different as the function of the extra heater position. Thus, the ANOVA of those fiber diameters is provided in [Figure 31].

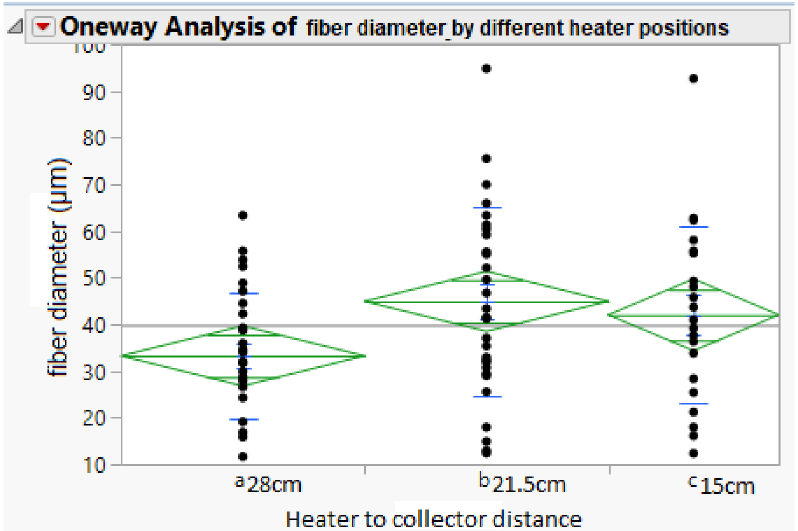

Oneway Anova

Summary of Fit

Rsquare	0.082132
Adj Rsquare	0.058597
Root Mean Square Error	17.70692
Mean of Response	39.86437
Observations (or Sum Wgts)	81

Analysis of Variance

Source	DF	Sum of Squares	Mean Square	F Ratio	Prob > F
Column 1	2	2188.343	1094.17	3.4898	0.0354*
Error	78	24455.719	313.53		
C. Total	80	26644.062			

Means for Oneway Anova

Level	Number	Mean	Std Error	Lower 95%	Upper 95%
a28cm	30	33.2494	3.2328	26.813	39.685
b21.5cm	30	44.9469	3.2328	38.511	51.383
c15cm	21	42.0536	3.8640	34.361	49.746

Ordered Differences Report

Level	- Level	Difference	Std Err Dif	Lower CL	Upper CL	p-Value
b21.5	a28	11.69750	4.571906	2.59553	20.79947	0.0124*
c15	a28	8.80417	5.037995	-1.22571	18.83405	0.0845
b21.5	c15	2.89333	5.037995	-7.13655	12.92321	0.5674

Figure 31. ANOVA and the pair t-test result of the diameter of fiber spun with different arrangement of heater located behind..

According to the statistic results, a higher ambient temperature is helping to produce thinner fibers (ANOVA for diameter between with and without extra heater scenarios, P-value = 0.0003). However, the fiber diameter change as the function of extra heater position is not always statistically different due to the high variance (only P-value for (21.5 cm VS 28 cm) < 0.05). Thus, to study this problem into detail, a chamber covering the system is desired for maintaining a higher ambient temperature, isolating the air flow, temperature, and humidity change in the lab from the spinning environment.

The chamber added into the system is a 1 m x 1 m x 1 m cubic 5-side chamber. Three vertical walls are made of wood and the top surface as well as the front door are made of transparent acrylics for observation purpose. All materials are chosen from electric insulation materials to avoid increasing the complexity of the electric field. The chamber is sitting on a rubber mat, isolating from the table surface.

In the in-chamber electrospinning system, a new heater (TempCo, ceramic coated housing double-tube IR lamp, 1000 W) is hanging above the source plate by 10 cm and controlled by the self-build PID temperature controller as well. A thermocouple is attached at 4 cm away from the heater surface.

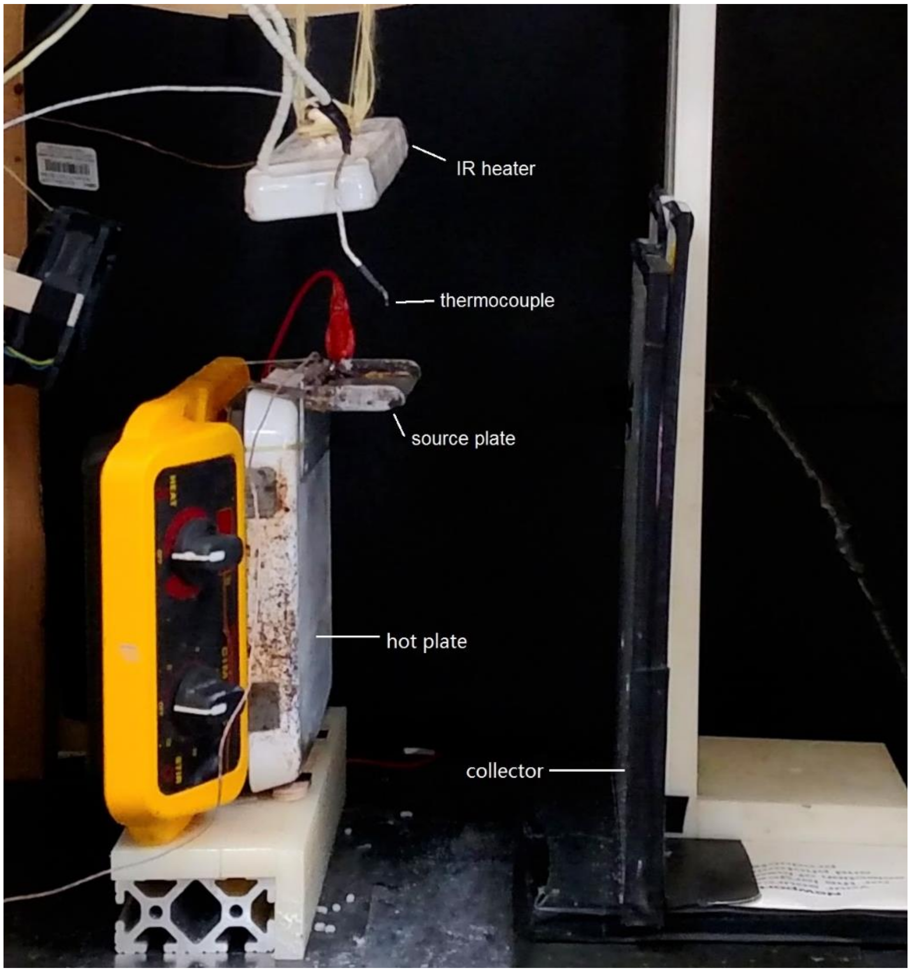

Figure 32. Photo of the setup at vertical configuration.

Setting the temperature over 200 °C is dangerous because it will burn the raw polymer. Sometimes, even the PE melt appears no problem by visually observation, the material will still become yellow after cooled down. 170 °C has been determined as a safe temperature. In the experiments, it worked with the vertical hot plate together as an assistant heating source. Due to the difficulty of measuring temperature in the closed chamber when the IR lamp is open, the following results in [Table 9] [Figure 33] are from the open-door experiments.

Table 9. Temperature records and fiber diameter about the upper extra heating.

configuration	temperature at 1cm (°C)	temperature at mid-point 5cm (°C)	fiber diameter (μm)	STD	Jet speed (m/min)
Only vertical Hot Plate	50	41	14	11	118
Vertical HotPlate+IR lamp	73	68	9	6	142

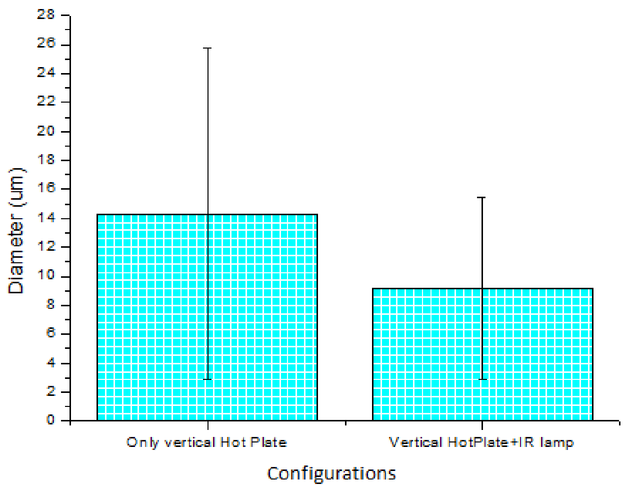

Figure 33. Fiber Diameter comparison between two heating configurations.

Oneway Analysis of average diameter by two heating configurations

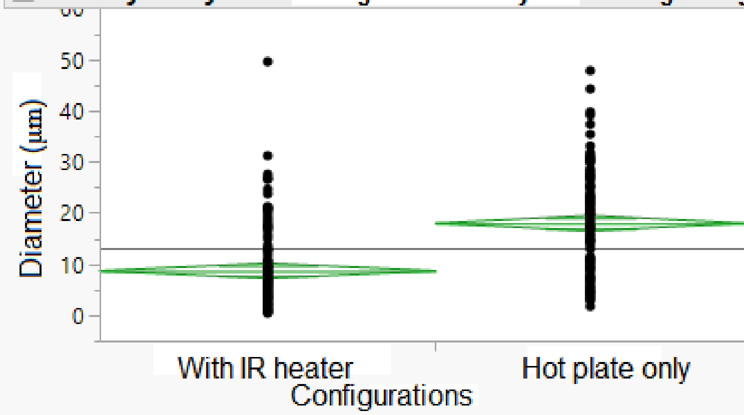

Oneway Anova

Summary of Fit

t Test

only vertical-10g close Duo new way
Assuming equal variances

Difference	9.3054	t Ratio	8.710932
Std Err Dif	1.0682	DF	307
Upper CL Dif	11.4074	Prob > |t|	<.0001*
Lower CL Dif	7.2034	Prob > t	<.0001*
Confidence	0.95	Prob < t	1.0000

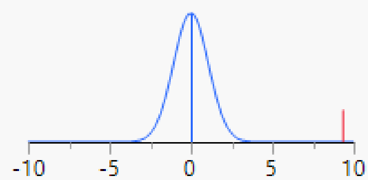

Analysis of Variance

Source	DF	Sum of Squares	Mean Square	F Ratio	Prob > F
Column 2	1	6677.232	6677.23	75.8803	<.0001*
Error	307	27015.038	88.00		
C. Total	308	33692.270			

Means for Oneway Anova

Level	Number	Mean	Std Error	Lower 95%	Upper 95%
10g close Duo new way	161	8.6906	0.73930	7.236	10.145
only vertical	148	17.9960	0.77109	16.479	19.513

Figure 34. ANOVA result of fiber diameter spun within the chamber or with open air setup.

According to the ANOVA test, as the P-value is < 0.001, those two diameter sets are very significant different which means a higher ambient temperature is helping to produce fibers with lower diameter. At the warmer spin environment, the obtained fiber is 36% thinner than the situation without heated environmental. The variation of the fiber diameter is also reduced from 11.424 µm to 6.297 µm. The jet speed is promoted by the warmer ambient temperature as well.

4.5. Air assist quenching and drawing

The multiple factors ANOVA shows that air flow also makes a significant difference in fiber diameter in the system. The airflow was introduced to enhance the drawing process in this electrospinning system, an air assist system was installed in this system in the later stage at the in-chamber system at vertical configuration. The photo is [Figure 32] and the black fan is at the left side. The subsystem consists an AC fan (Diameter 12 cm, 12 V) and a 120 V to 12 V variable electric transformer (UNITRON, P 117V). The transformer could output the AC power from 0 to 12 V. The fan doesn't have the function of generating heat.

The fan was running at 8 V in this study and the air flow rate was 860 cm^3/s at that voltage. The airflow has been tested that it is not strong enough to break the microfibers spun by this system so the fibers could be drawn instead of being broken before solidified.

The jets in the air assisted system are supposed to solidify earlier than the normal condition because the overall environment was cooler. Theoretically, this will lead to a thicker fiber diameter for the shorter drawing process. However, the fiber diameter comparison is shown in [Figure 35]. The airflow is helping to get statistical thinner fibers (P-value < 0.001 by ANOVA).

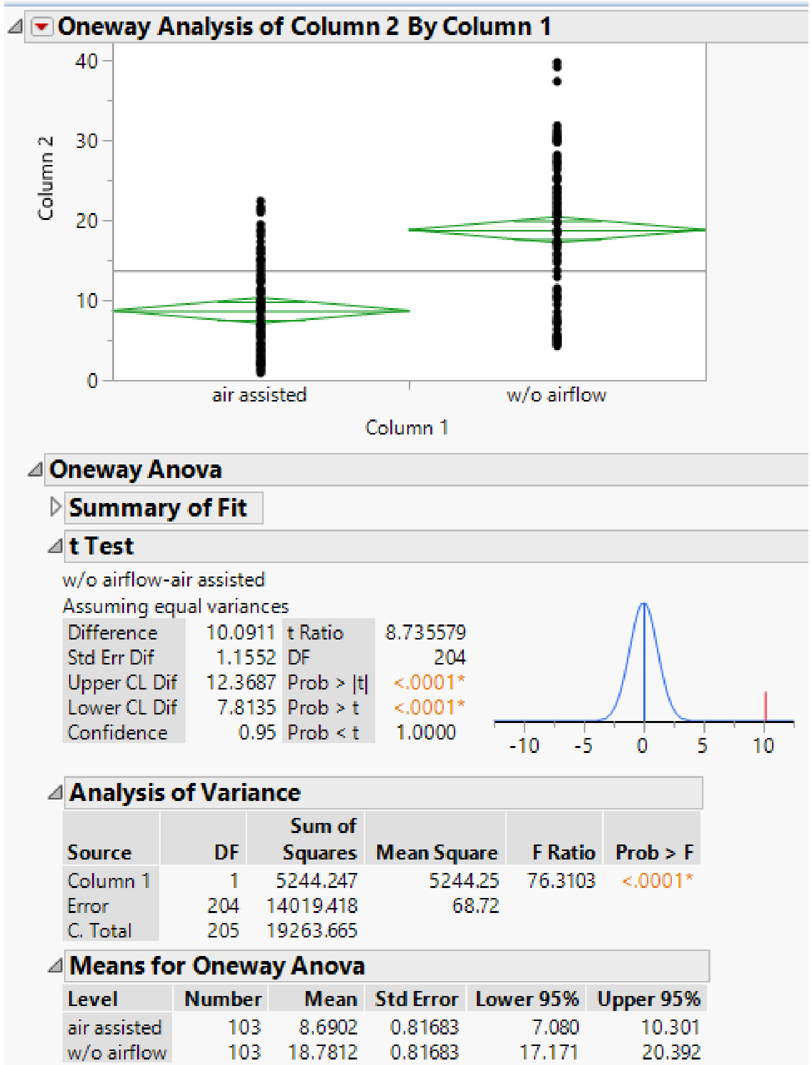

Difference	10.0911	t Ratio	8.735579
Std Err Dif	1.1552	DF	204
Upper CL Dif	12.3687	Prob > |t|	<.0001*
Lower CL Dif	7.8135	Prob > t	<.0001*
Confidence	0.95	Prob < t	1.0000

Source	DF	Sum of Squares	Mean Square	F Ratio	Prob > F
Column 1	1	5244.247	5244.25	76.3103	<.0001*
Error	204	14019.418	68.72		
C. Total	205	19263.665			

Level	Number	Mean	Std Error	Lower 95%	Upper 95%
air assisted	103	8.6902	0.81683	7.080	10.301
w/o airflow	103	18.7812	0.81683	17.171	20.392

Figure 35. ANOVA of fiber diameters: with/without air assist system.

The jet number has been counted and plotted in [Figure 36]. With airflow, the jet number is less than the process without air assist system. However, if counting the overall jet speed, the difference is not big (1616 m/min for air assist VS 1880 m/min for normal condition).

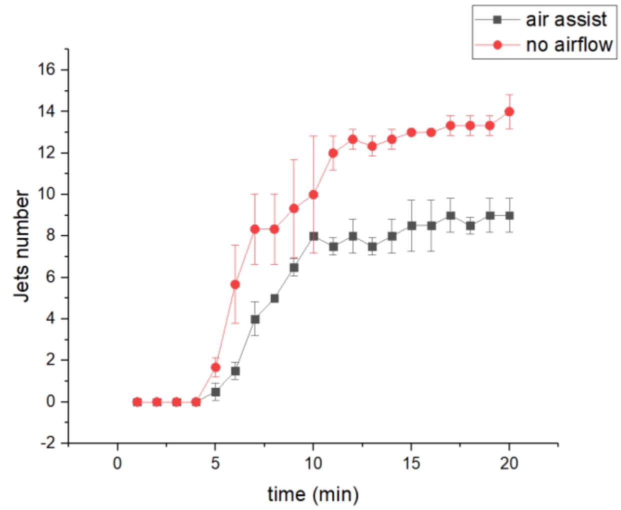

Figure 36. The jet number counting during the spinning process with/without air.

The Taylor cone usually has a length between 1 - 10 mm in this study so the first 10 mm of the spin line might affect the generation of Taylor cone the most. Due to the air stream, the heat generated by the hot plate surface has been transferred more to the first temperature checkpoint at 1 cm. In a longer distance, the spin line temperature with extra airflow is about 8 °C lower than the stable air ambient because of a faster thermal convection. Temperature along the spin line is shown as [Figure 37].

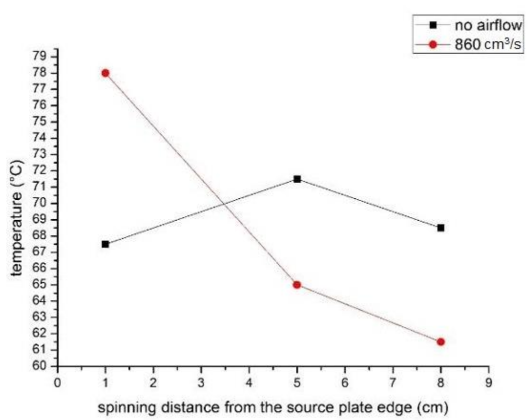

Figure 37. Temperature gradience along the spin line.

The result of this study indicates that the first area is the most temperature sensitive part that helping to perform stronger drawing process. The hotter temperature at the beginning part is more effective in producing thinner fibers because there is area that jets still remain at high temperature and still in melt phase. In the later part, the viscosity increased a lot, if not in solid status and not sensitive to the drawing force.

The conclusion is, as a function of airflow, the fiber could be thinner as long as the initial area is not cooler than before. The jet speed was also increased from 118 to 202 m/min, almost double of the former. Although the jet number has been decreased, the jet speed is not dropping much that the air assist subsystem has the value to continue study.

4.6. Thickness of polymer melt layer

As the finite element analysis result in 4.1 [Figure 14] shows that at 1 mm above the spinning edge, the electric intensity has dropped to 20% from the center already. It is interesting to know if a thicker polymer melt layer could still be spun effectively by the electric field. In this study, 10 g DOW ASPUN 6850A PE powder was placed on the source plate every time.

The density of 6850A is 0.955 g/cm^3. The volume of 10 g PE is:

$$volume = mass / density$$

$$= 10 / 0.955$$

$$= 10.471\ cm^3$$

The inner size of the source plate is 13.6 cm x 4.6 cm, so the thickness of the polymer melt should be:

$$H = V/(L*W)$$

$$= 10.471 / (13.6*4.6)$$

$$=0.167 \text{ cm } (1.67 \text{ mm})$$

Assuming the electric intensity > 2 x 10^6 kV is considered “strong” then 40% of the polymer cross-section is outside the strong field. If the source PE is 15 g, 60% of the cross-section is out of the strong electric field. Too much area beyond the strong electric field might results in a bad cone forming process.

To verify this assumption, experiments with the gradience of source polymer is shown in [Table 10] [Figure 38]. The result was collected at early stage of this study with an open spinning system at horizontal configuration. This is the reason that fiber diameters are relatively large. However, due to the significant effect of the polymer layer thickness. The result is still meaningful to discuss.

Table 10. The fiber diameter comparison in different thickness of source material.

PE mass (g)	Thickness (mm)	Fiber diameter (µm)	STD
12.5	2.1	130	19
10	1.7	92	20
7.5	1.3	59	19
5	0.8	unable to spin	N/A

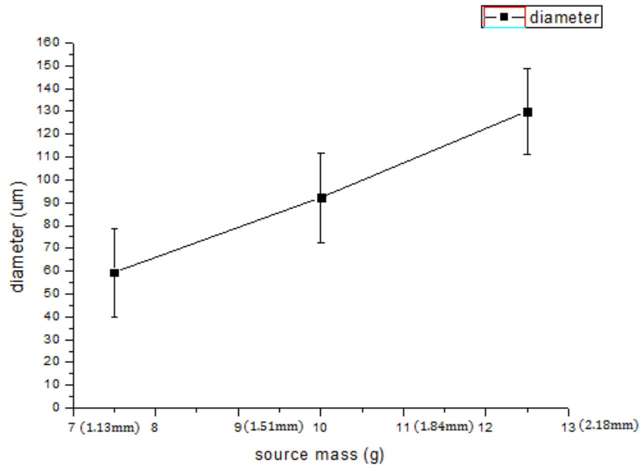

Figure 38. Fiber diameter change against the thickness of polymer source.

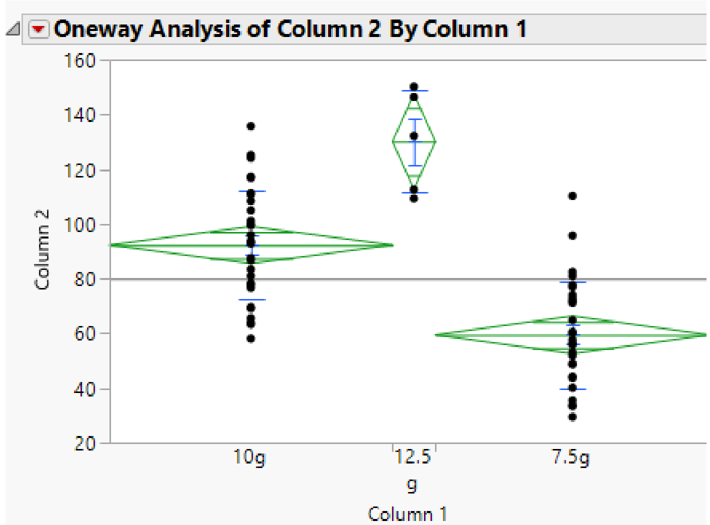

Oneway Anova

Summary of Fit

Rsquare	0.549829
Adj Rsquare	0.536391
Root Mean Square Error	19.47945
Mean of Response	79.99236
Observations (or Sum Wgts)	70

Analysis of Variance

Source	DF	Sum of Squares	Mean Square	F Ratio	Prob > F
Column 1	2	31051.186	15525.6	40.9162	<.0001*
Error	67	25423.074	379.4		
C. Total	69	56474.260			

Figure 39. ANOVA result of fiber diameter spun at different polymer melt layer.

First three rows are implicit. As the polymer melt is getting thicker, the fiber diameter is getting greater accordingly in a linear trend. The diameter difference is statistical very significant different as the $P < 0.0001$. The observation shows that the Taylor cone was bigger at the edge of thicker polymer layer, resulting thicker fibers. Another explanation is the electric intensity is diluted by the larger stress area, so the force applied to the spinning edge is not condensed enough to draw the fiber into smaller thickness.

Based on this assumption, the thinnest polymer melt at 5 g should spin the smallest fibers due to the most concentrated electric field. However, it was unable to spin on the contrary.

In the recorded spinning video, some jets were continue getting thinner and died during the process. The cone size was decreased with the jet diameter decrease in the process. At the breaking point, the surface tension overcame the electric repulsion force inside the too small cone and pushed the cone back to a flat surface.

Another reason could be the surface tension of the polymer melt that it is shrinking the entire surface. For a less volume of polymer layer on the plate, it is easier to move all melt at the edge that there is no material to spin.

This relationship gives an inspiration of the dynamic control of the fiber diameter. If the tilt angle of the source plate is controlled, the fiber diameter could be adjusted without any stop because the movement of polymer layer driven by gravity will change the cross-section area thickness at the edge. This is practical in the application because the preheating and jets initiating usually take more than 20 minutes on average. In a larger scale production, because the production line might start from source material and end with packaging, the stop is an annoying error disturbing the whole line that should be avoided with great efforts.

An experiment was done, and the result is in [Table 11]:

Table 11. The change of fiber diameter as the function of source plate angle.

angle	fiber diameter (μm)
2-degree downhill tilled	23
level	11

This is an encouragement for future optimization in this direction.

5. CONCLUSIONS

After experiments have been conducted based on the organization in the roadmap, [Figure 40], effects and explanation of the parameters influencing the spinning process could be made and stated in [Table 12].

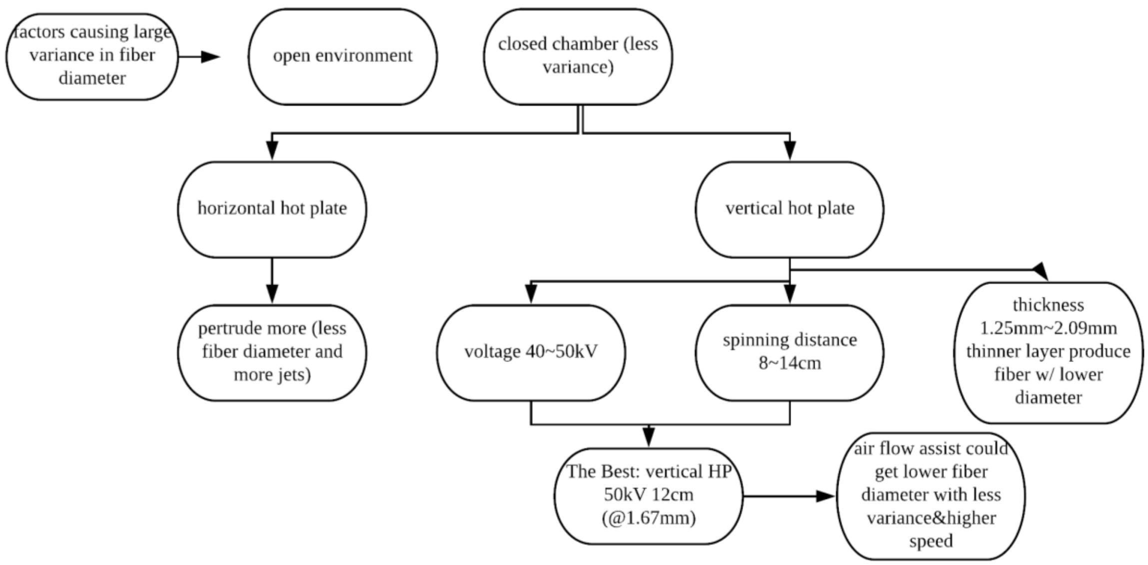

Figure 40. The roadmap of this study.

Table 12. Effects of parameters and explanations.

Parameter	Effect	Explanation
Source plate position and electric field	In horizontal configuration, more protrusion results in a stronger electric field.	The hot plate under the source plate is acting a negative factor of the electric field distribution. Stronger E promotes production of fibers with smaller diameter and higher jet speed.
Orientation of the hot plate	Fiber diameter is smaller when the hot plate is positioned vertically rather than at horizontally.	Vertical configuration provides the longest protruding distance of the source plate edge which gives a stronger electric field. The heating surface of the hot plate is directed to the spinning area, increasing the ambient temperature. This is a combined effect of stronger electric intensity and warmer ambient temperature results in smaller fiber diameters and higher jet speed.
Voltage and distance	As expected, higher voltage and smaller working distance produces thinner fibers and higher throughput rate. When the electric intensity is too high, it will breakdown resulting in a discharge.	Electric intensity increases as voltage increases and working distance decreases. Finite element model was validated experimentally under different spinning conditions.
Ambient temperature	Fiber diameter decreased when spun at a warmer ambient temperature.	The viscosity of the jet is lower when at higher ambient temperature. This enables the jet to remain more "fluid" at distances closer to the collector resulting in smaller fiber diameters and higher jet speed.

Table 13. Continue.

Airflow	Low airflow helps to transfer the heat from the hot plate to the spinning area which is promotes Taylor cone formation. High airflow will suppress the formation of Taylor cones.	Low airflow blows warmer air to the spinning region, which lowers the polymer viscosity at the plate edge, thereby promoting Taylor cone formation. High airflow can disrupt jet formation and create breaks therefore lowering the overall jet speed.
Open/ close environment	Open spinning environment has larger variance and not significant difference in fiber diameter as the function of temperature change.	Thermal convection near the system is not negligible. In the open environment air flow in the lab is disrupting the spinning process and should be avoided. This can be remedied by using the closed system.
Polymer layer thickness	Thinner polymer melt layer on source plate will produce smaller fibers diameters. There is a lower limit to the molten layer, below which jets will not initiate and no fibers will be formed.	The formation of the Taylor cone is based on the overall cross-section of the fluid. Thicker fluid layers result in larger cones and therefore thicker fibers. If the fluid layer is too thin, cones will not be formed and jets will not be initiated.
	Tilting angle of source plate can control the fiber diameter without stopping spinning.	This is an alternate way to control the fluid layer at the spinning edge. Results are inclusive and not consistent.

The quality assurance study was conducted at the start of this study, made several measures to decrease errors and mistakes in the whole experiment process. A chamber was built to provide a stable, isolating, controllable small environment for electrospinning.

During the quality improving process, the protruding distance effect of the source plate was recognized that the longer distance will perform a lower fiber diameter and more jet number. Based on the observation, a detailed model of the melt electrical spinning system was built and the electric field distribution around the source plate was analyzed by the finite element analysis (FEA). FEA results proved the assumption that a longer protruding distance provides a stronger electric field near the edge of source plate and this is promoting the spinning process. Thus, a new configuration of the unconfined edge melt electrospinning that gives a longest protruding distance, the vertical hot plate version, was designed and showed a better performance in fiber quality, jet number and jet speed.

The ideal electric field intensity range is specified. The voltage range is 40-50 kV and the distance range is 8-12 cm. Within the proper range, the fiber diameter decreases as the function of increasing spinning voltage and decreasing working distance.

The hotter ambient temperature of the spinning system is helpful to produce thinner fibers at a faster speed with lower variance. The most useful part is the area close to the source plate, where Taylor cones located.

Polymer melt layer at the edge should have proper thickness according to the intensity distribution. This study shows that thinner polymer layer could produce thinner fibers when other parameters are constant. However, there is a lower limit for the polymer layer thickness because of the distribution of the polymer melt layer is affected by the surface tension. The material at the edge has a potential to move to the center and will be not enough material remaining at the edge for a too thin layer.

Air flow applied to jets decreases the fiber diameter at the speed of 860 cm^3/s. The cooling effect of the air flow at the middle to end section is tolerable as long as the first section remains hot.

FUTURE WORK

Due to the time and instrument restriction, a few works are suggested for the future researchers.

A robust and accurate temperature measuring system is desired for the temperature effects. For instance, the vertical configuration may not just be promoted by the electric field but also the thermal radiation from the collector-facing hot plate.

The diameter controller by tilt angle is also an interesting part to add in the system. The electric field change by the tilt angle should be studied as well.

An ideal airflow relates with the tradeoff between the warmer temperature at the beginning and a cooler temperature at the middle to end part, the drawing force and the fragile melt jet is a top requires efforts.

The molecular weight loss of the produced fibers and the mechanical property of the fibers could also be a topic to study. Some preliminary experiments have shown that the fiber has up to meters long breaking length.

PUBLICATION BIBLIOGRAPHY

Brown, Toby D.; Dalton, Paul D.; Hutmacher, Dietmar W. (2016): Melt electrospinning today: An opportune time for an emerging polymer process. In *Progress in Polymer Science* 56, pp. 116–166. DOI: 10.1016/j.progpolymsci.2016.01.001.

Cai, Shaobo; Xu, Helan; Jiang, Qiuran; Yang, Yiqi (2013): Novel 3D electrospun scaffolds with fibers oriented randomly and evenly in three dimensions to closely mimic the unique architectures of extracellular matrices in soft tissues: fabrication and mechanism study. In *Langmuir : the ACS journal of surfaces and colloids* 29 (7), pp. 2311–2318. DOI: 10.1021/la304414j.

Cooley, John F. (1903): Electrical method of dispersing fluids. UNITED STATES, 11/3/1903 (US745276A).

Dalton, Paul; Grafahrend, Dirk; Klinkhammer, Kristina; Klee, Doris; Möller, Martin (2007): Electrospinning of polymer melts: Phenomenological observations. In *Polymer* 48 (23), pp. 6823–6833. DOI: 10.1016/j.polymer.2007.09.037.

Deng, Rongjian; Liu, Yong; Ding, Yumei; Xie, Pengcheng; Luo, Lu; Yang, Weimin (2009): Melt electrospinning of low-density polyethylene having a low-melt flow index. In *J. Appl. Polym. Sci.* 114 (1), pp. 166–175. DOI: 10.1002/app.29864.

Dosunmu, O. O.; Chase, G. G.; Kataphinan, W.; Reneker, D. H. (2006): Electrospinning of polymer nanofibres from multiple jets on a porous tubular surface. In *Nanotechnology* 17 (4), pp. 1123–1127. DOI: 10.1088/0957-4484/17/4/046.

Farrugia, Brooke L.; Brown, Toby D.; Upton, Zee; Hutmacher, Dietmar W.; Dalton, Paul D.; Dargaville, Tim R. (2013): Dermal fibroblast infiltration of poly(ε-caprolactone) scaffolds fabricated by melt electrospinning in a direct writing mode. In *Biofabrication* 5 (2), p. 25001. DOI: 10.1088/1758-5082/5/2/025001.

Hoffstetter, M.; Wintermantel, E. (2010): MESO fiber - a novel approach to reinforce micro parts. MESO Faser - ein nauartiger Ansatz zur Verstärkung von Mikrobauteilen. In *Mat.-wiss. u. Werkstofftech.* 41 (12), pp. 1011–1018. DOI: 10.1002/mawe.201000702.

Hu, Xiuli; Liu, Shi; Zhou, Guangyuan; Huang, Yubin; Xie, Zhigang; Jing, Xiabin (2014): Electrospinning of polymeric nanofibers for drug delivery applications. In *Journal of controlled release : official journal of the Controlled Release Society* 185, pp. 12–21. DOI: 10.1016/j.jconrel.2014.04.018.

Huang, Zheng-Ming; Zhang, Y.-Z.; Kotaki, M.; Ramakrishna, S. (2003): A review on polymer nanofibers by electrospinning and their applications in nanocomposites. In *Composites Science and Technology* 63 (15), pp. 2223–2253. DOI: 10.1016/S0266-3538(03)00178-7.

Hung, Chi-Ho; Leung, Wallace Woon-Fong (2011): Filtration of nano-aerosol using nanofiber filter under low Peclet number and transitional flow regime. In *Separation and Purification Technology* 79 (1), pp. 34–42. DOI: 10.1016/j.seppur.2011.03.008.

Kaiser, Kenneth L. (2006): Electrostatic discharge. Boca Raton, Fla., London: CRC.

Kapllani, Alda; Dillard, Caitlin; Washington, Katherine E.; Biewer, Michael C.; Stefan, Mihaela C.; Kalra, Vibha (2014): Self-Assembly of Poly(3-hexylthiophene)-block -poly(γ-benzyl- L -glutamate) within Solution-Cast Films and Nanofibers. In *Macromol. Mater. Eng.* 299 (12), pp. 1484–1493. DOI: 10.1002/mame.201400148.

Kim, Jong-sang; Reneker, Darrell H. (1999): Mechanical properties of composites using ultrafine electrospun fibers. In *Polym. Compos.* 20 (1), pp. 124–131. DOI: 10.1002/pc.10340.

Larrondo, L.; St. John Manley, R. (1981): Electrostatic fiber spinning from polymer melts. I. Experimental observations on fiber formation and properties. In *J. Polym. Sci. Polym. Phys. Ed.* 19 (6), pp. 909–920. DOI: 10.1002/pol.1981.180190601.

Li, Haoyi; Chen, Hongbo; Zhong, Xiangfeng; Wu, Weifeng; Ding, Yumei; Yang, Weimin (2014a): Interjet distance in needleless melt differential electrospinning with umbellate nozzles. In *J. Appl. Polym. Sci.* 131 (15), n/a-n/a. DOI: 10.1002/app.40515.

Li, Haoyi; Wu, Weifeng; Bubakir, Mahmoud M.; Chen, Hongbo; Zhong, Xiangfeng; Liu, Zhaoxiang et al. (2014b): Polypropylene fibers fabricated via a needleless melt‐electrospinning device for marine oil‐spill cleanup. In *Journal of Applied Polymer Science* 131 (7).

Liang, Hai-Wei; Guan, Qing-Fang; Chen, Li-Feng; Zhu, Zhu; Zhang, Wen-Jun; Yu, Shu-Hong (2012): Macroscopic-scale template synthesis of robust carbonaceous nanofiber hydrogels and aerogels and their applications. In *Angewandte Chemie (International ed. in English)* 51 (21), pp. 5101–5105. DOI: 10.1002/anie.201200710.

Liu, Yong; Deng, Rongjian; Hao, Mingfeng; Yan, Hua; Yang, Weimin (2010): Orthogonal design study on factors effecting on fibers diameter of melt electrospinning. In *Polym Eng Sci* 50 (10), pp. 2074–2078. DOI: 10.1002/pen.21753.

Liu, Yong; He, J-H (2007): Bubble electrospinning for mass production of nanofibers. In *International Journal of Nonlinear Sciences and Numerical Simulation* 8 (3), pp. 393–396.

Lv, Chade; Chen, Gang; Sun, Jingxue; Yan, Chunshuang; Dong, Hongjun; Li, Chunmei (2015): One-dimensional Bi 2 O 3 QD-decorated BiVO 4 nanofibers: electrospinning synthesis, phase separation mechanism and enhanced photocatalytic performance. In *RSC Adv.* 5 (5), pp. 3767–3773. DOI: 10.1039/C4RA11065J.

Lyons, Jason; Li, Christopher; Ko, Frank (2004): Melt-electrospinning part I: processing parameters and geometric properties. In *Polymer* 45 (22), pp. 7597–7603. DOI: 10.1016/j.polymer.2004.08.071.

Niu, Haitao; Lin, Tong; Wang, Xungai (2009): Needleless electrospinning. I. A comparison of cylinder and disk nozzles. In *J. Appl. Polym. Sci.* 114 (6), pp. 3524–3530. DOI: 10.1002/app.30891.

Ogata, Nobuo; Yamaguchi, Shinji; Shimada, Naoki; Lu, Gang; Iwata, Toshiharu; Nakane, Koji; Ogihara, Takashi (2007): Poly(lactide) nanofibers produced by a melt-electrospinning system with a laser melting device. In *J. Appl. Polym. Sci.* 104 (3), pp. 1640–1645. DOI: 10.1002/app.25782.

Ondarcuhu, T.; Joachim, C. (1998): Drawing a single nanofibre over hundreds of microns. In *EPL (Europhysics Letters)* 42 (2), p. 215.

Roman, Michael P.; Thoppey, Nagarajan M.; Gorga, Russell E.; Bochinski, Jason R.; Clarke, Laura I. (2013): Maximizing Spontaneous Jet Density and Nanofiber Quality in Unconfined Electrospinning: The Role of Interjet Interactions. In *Macromolecules* 46 (18), pp. 7352–7362. DOI: 10.1021/ma4013253.

Schmid, Christian F.; Switzer, Leonard H.; Klingenberg, Daniel J. (2000): Simulations of fiber flocculation: Effects of fiber properties and interfiber friction. In *Journal of Rheology* 44 (4), pp. 781–809. DOI: 10.1122/1.551116.

Subbiah, Thandavamoorthy; Bhat, G. S.; Tock, R. W.; Parameswaran, S.; Ramkumar, S. S. (2005): Electrospinning of nanofibers. In *J. Appl. Polym. Sci.* 96 (2), pp. 557–569. DOI: 10.1002/app.21481.

Sun, Daoheng; Chang, Chieh; Li, Sha; Lin, Liwei (2006): Near-field electrospinning. In *Nano letters* 6 (4), pp. 839–842. DOI: 10.1021/nl0602701.

W. L. Peticolas and J. M. Watkins (1957): The Molecular Structure of Polyethylene. VII. Melt Viscosity and the Effect of Molecular Weight and Branching[1].

Wang, Qingqing; Curtis, Colin K.; Thoppey, Nagarajan Muthuraman; Bochinski, Jason R.; Gorga, Russell E.; Clarke, Laura I. (2014): Unconfined, melt edge electrospinning from multiple, spontaneous, self-organized polymer jets. In *Mater. Res. Express* 1 (4), p. 45304. DOI: 10.1088/2053-1591/1/4/045304.

Xing, Xiaobo; Wang, Yuqing; Li, Baojun (2008): Nanofibers drawing and nanodevices assembly in poly(trimethylene terephthalate). In *Opt. Express* 16 (14), p. 16815. DOI: 10.1364/OE.16.016815.

Zhmayev, Eduard; Cho, Daehwan; Joo, Yong Lak (2010): Nanofibers from gas-assisted polymer melt electrospinning. In *Polymer* 51 (18), pp. 4140–4144. DOI: 10.1016/j.polymer.2010.06.058.